



UNIVERSIDAD DE INVESTIGACIÓN DE TECNOLOGÍA EXPERIMENTAL YACHAY

Escuela de Ciencias Químicas e Ingeniería

SYNTHESIS AND CHARACTERIZATION OF CHEMICALLY CROSS LINKED CARBOXYMETHYL CELLULOSE/CHITOSAN COMPOSITE HYDROGELS

Trabajo de integración curricular presentado como requisito para la
obtención del título de Petroquímico

Autor:

Luis Alberto Calderón Salas

Tutores:

MSc. Lola De Lima Eljuri

Ph.D Manuel Caetano Sousa

Urcuquí, Abril 2021

SECRETARÍA GENERAL
(Vicerrectorado Académico/Cancillería)
ESCUELA DE CIENCIAS QUÍMICAS E INGENIERÍA
CARRERA DE PETROQUÍMICA
ACTA DE DEFENSA No. UITEY-CHE-2021-00012-AD

A los 23 días del mes de junio de 2021, a las 16:00 horas, de manera virtual mediante videoconferencia, y ante el Tribunal Calificador, integrado por los docentes:

Presidente Tribunal de Defensa	Dra. GONZALEZ VAZQUEZ, GEMA , Ph.D.
Miembro No Tutor	Dr. SAUCEDO VAZQUEZ, JUAN PABLO , Ph.D.
Tutor	Mgs. DE LIMA ELJURI, LOLA MARIA

El(la) señor(ita) estudiante CALDERON SALAS, LUIS ALBERTO, con cédula de identidad No. 1003741525, de la ESCUELA DE CIENCIAS QUÍMICAS E INGENIERÍA, de la Carrera de PETROQUÍMICA, aprobada por el Consejo de Educación Superior (CES), mediante Resolución RPC-SO-39-No.456-2014, realiza a través de videoconferencia, la sustentación de su trabajo de titulación denominado: SYNTHESIS AND CHARACTERIZATION OF CHEMICALLY CROSSLINKED CARBOXYMETHYL CELLULOSE/CHITOSAN COMPOSITE HYDROGEL, previa a la obtención del título de PETROQUÍMICO/A.

El citado trabajo de titulación, fue debidamente aprobado por el(los) docente(s):

Tutor	Mgs. DE LIMA ELJURI, LOLA MARIA
--------------	---------------------------------

Y recibió las observaciones de los otros miembros del Tribunal Calificador, las mismas que han sido incorporadas por el(la) estudiante.

Previamente cumplidos los requisitos legales y reglamentarios, el trabajo de titulación fue sustentado por el(la) estudiante y examinado por los miembros del Tribunal Calificador. Escuchada la sustentación del trabajo de titulación a través de videoconferencia, que integró la exposición de el(la) estudiante sobre el contenido de la misma y las preguntas formuladas por los miembros del Tribunal, se califica la sustentación del trabajo de titulación con las siguientes calificaciones:

Tipo	Docente	Calificación
Tutor	Mgs. DE LIMA ELJURI, LOLA MARIA	10,0
Presidente Tribunal De Defensa	Dra. GONZALEZ VAZQUEZ, GEMA , Ph.D.	10,0
Miembro Tribunal De Defensa	Dr. SAUCEDO VAZQUEZ, JUAN PABLO , Ph.D.	9,8

Lo que da un promedio de: **9.9 (Nueve punto Nueve)**, sobre 10 (diez), equivalente a: **APROBADO**

Para constancia de lo actuado, firman los miembros del Tribunal Calificador, el/la estudiante y el/la secretario ad-hoc.

Certifico que en cumplimiento del Decreto Ejecutivo 1017 de 16 de marzo de 2020, la defensa de trabajo de titulación (o examen de grado modalidad teórico práctica) se realizó vía virtual, por lo que las firmas de los miembros del Tribunal de Defensa de Grado, constan en forma digital.

CALDERON SALAS, LUIS ALBERTO
Estudiante

GEMA GONZALEZ Vazquez
GONZALEZ VAZQUEZ
DNI: 2021 0707 791444-0202

Dra. GONZALEZ VAZQUEZ, GEMA , Ph.D.
Presidente Tribunal de Defensa

AUTORÍA

Yo, **LUIS ALBERTO CALDERÓN SALAS**, con cédula de identidad 1003741525, declaro que las ideas, juicios, valoraciones, interpretaciones, consultas bibliográficas, definiciones y conceptualizaciones expuestas en el presente trabajo; así como, los procedimientos y herramientas utilizadas en la investigación, son de absoluta responsabilidad de el/la autora (a) del trabajo de integración curricular. Así mismo, me acojo a los reglamentos internos de la Universidad de Investigación de Tecnología Experimental Yachay.

Urcuquí, abril de 2021.



Luis Alberto Calderón Salas

CI:1003741525

AUTORIZACIÓN DE PUBLICACIÓN

Yo, **LUIS ALBERTO CALDERÓN SALAS**, con cédula de identidad 1003741525, cedo a la Universidad de Tecnología Experimental Yachay, los derechos de publicación de la presente obra, sin que deba haber un reconocimiento económico por este concepto. Declaro además que el texto del presente trabajo de titulación no podrá ser cedido a ninguna empresa editorial para su publicación u otros fines, sin contar previamente con la autorización escrita de la Universidad.

Asimismo, autorizo a la Universidad que realice la digitalización y publicación de este trabajo de integración curricular en el repositorio virtual, de conformidad a lo dispuesto en el Art. 144 de la Ley Orgánica de Educación Superior

Urcuquí, abril de 2021.



Luis Alberto Calderón Salas

CI:1003741525

Dedicatoria

El presente trabajo de investigación dedico a mi madre, tía y principalmente Dios, por haberme dado inspiración y fuerza para obtener un sueño más.

A todas las personas que me han apoyado y han hecho que el trabajo se desarrolle con éxito en especial a aquellos que nos abrieron las puertas y compartieron sus conocimientos.

Luis Alberto Calderón Salas

Agradecimientos

Agradezco a la Escuela de Ciencias Químicas e Ingeniería de la Universidad Yachay Tech, por haber compartido sus conocimientos a lo largo del desarrollo de mi profesión, de manera especial, a mis tutores MSc. Lola De Lima Eljuri y Ph.D Caetano Sousa Manuel por el desarrollo de nuestro proyecto de investigación quienes me han guiado con sus conocimientos y su rectitud como docentes. También a los profesores con los cuales he tenido la oportunidad de compartir momentos, enseñanzas además de ser fuentes de inspiración en áreas de investigación. Agradecimientos especiales a Ph.D. Kamil Makowski por sus conocimientos en química orgánica y manejo de programas químicos y Ph.D. Carlos Reinoso por los estudios en X-ray Photoelectron Spectroscopy quienes facilitaron el desarrollo de este trabajo de investigación.

Luis Alberto Calderón Salas

RESUMEN

Este trabajo se centra en la preparación verde de composites hidrogeles con propiedades mecánicas y químicas que los hacen adecuados para aplicaciones de la vida real. Los polimorfos de quitosano (α y β) se combinaron por separado con carboximetilcelulosa para crear hidrogeles compuestos que presentan simultáneamente grupos carboxilato, hidroxilo y amina. Ácido cítrico fue usado para promover la reticulación química y se usó glicerol como plastificante. La caracterización fisicoquímica, morfológica y térmica de los hidrogeles compuestos se realizó mediante estudio de hinchamiento, Espectrometría Infrarroja por Transformada de Fourier, Calorimetría Diferencial de Barrido, Difracción de Rayos X en Polvo, Espectroscopia Foteoelectrónica de Rayos X, Resonancia Magnética Nuclear, Microscopía Electrónica de Barrido y Estereomicroscopía. Los hidrogeles hinchados presentaron un aspecto liso y homogéneo, con presencia de macroporos y comportamiento elástico. Sin embargo, una vez que se secaron, el material perdió su elasticidad y se volvió rígido. En el proceso de hinchamiento, el hidrogel compuesto con el porcentaje de velocidad de hinchamiento de equilibrio más alto alcanzó el 98% a las 24 h. Los estudios espectroscópicos confirman el logro de la reticulación química y física. La reticulación química consiste en la formación de enlaces amida y éster promovidos por la reacción del ácido cítrico con quitosano y carboximetilcelulosa, respectivamente. En el caso de la reticulación física, la confirmación se obtuvo por la presencia de interacciones COO^- y NH_3^+ . Se propuso una estructura molecular media de hidrogeles compuestos.

Palabras clave: reticulación química, compuestos, hidrogeles, esponjas y forma de memoria.

ABSTRACT

This work focuses on green preparation of composite hydrogels with mechanical and chemical properties that make them suitable for real life applications. Polymorphs of chitosan (α and β) were combined separately with carboxymethyl cellulose to create composite hydrogels that present simultaneously carboxylate, hydroxyl, and amine groups. Citric acid was used to promote chemical crosslink and glycerol was used as plasticizer. Physicochemical, morphological, and thermal characterization of composite hydrogels were carried on by means of swelling study, Fourier Transform Infrared Spectrometry, Differential Scanning Calorimetry, X-ray Powder Diffraction, X-Ray Photoelectron Spectroscopy, Nuclear Magnetic Resonance, Scanning Electron Microscopy, and stereomicroscopy. The swelled hydrogels presented a smooth and homogeneous appearance, with the presence of macropores and elastic behavior. However, once they were dried, the material lost its elasticity and became rigid. In the swelling process, the composite hydrogel with the highest equilibrium swelling rate percentage reached 98% at 24 h. Spectroscopical studies confirm the achievement of chemical and physical crosslinking. The chemical crosslinking consists of the formation of amide and ester bonds promoted by citric acid reaction with chitosan and carboxymethyl cellulose, respectively. In the case of physical crosslinking, confirmation was obtained by the presence of COO^- and NH_3^+ interactions. An average molecular structure of composite hydrogels was proposed.

Key Words: chemical crosslinking, composites, hydrogels, sponges, and memory shape.

ABBREVIATIONS AND ACRONYMS

CMC	Sodium Carboxymethyl Cellulose
CH	Chitosan
GL	Glycerol
CA	Citric Acid
DA	Degree of acetylation
FTIR-ATR	Transform Infrared Spectroscopy - Attenuated Total Reflectance
DSC	Differential Scanning Calorimeter
XRD	X-ray Powder Diffraction
XPS	X-ray Photoelectron Spectroscopy
LF ¹H NMR	Low-Field ¹ H Nuclear Magnetic Resonance
SEM	Scanning Electron Microscopy
TEMPO	2,2,6,6-tetramethylpiperidine-1-oxyl radical

TABLE OF CONTENTS

CONTENT	1
1 INTRODUCTION-JUSTIFICATION	1
2 PROBLEM STATEMENT	2
3 GENERAL AND SPECIFIC OBJECTIVES	3
3.1 General objective	3
3.2 Specific objectives	3
4 THEORETICAL BACKGROUND.....	4
4.1 Hydrogels.....	4
4.1.1 History and importance of hydrogels.....	4
4.1.2 Hydrogels Definition	4
4.1.3 Types of hydrogels in accordance with crosslinking.....	4
4.1.4 Hydrogel classification according to the type of application.....	4
4.2 Cellulose	5
4.2.1 Cellulose polymorphisms.....	6
4.2.2 Nanocellulose.....	6
4.2.3 Crystalline nanocellulose	6
4.2.4 Nanowhiskers.....	6
4.3 Carboxymethyl cellulose	7
4.3.1 Synthesis of Carboxymethylcellulose.....	7
4.3.2 Hydrogels based on CMC, CA, and other compounds.....	8
4.4 Chitosan	9
4.4.1 Types of chitosan	9
4.4.2 Films and hydrogels of chitosan	9

4.5	Sponges based on chitosan and cellulose.....	10
4.6	Bioengineered hydrogels	11
4.6.1	Hydrogels for skin tissue engineering.....	11
4.6.2	Hydrogels artificial skins	12
4.6.3	Hydrogels regeneration of skin tissue.....	12
4.6.4	Hydrogels with modulated release of drugs for skin	13
4.6.5	Hydrogels for bone and cartilage replacement	13
4.7	Characterization Techniques.....	15
4.7.1	Swelling Ratio.....	15
4.7.2	Fourier Transform Infrared Spectroscopy-Attenuated Total Reflectance	15
4.7.3	Differential Scanning Calorimetry.....	16
4.7.4	X-Ray Diffraction	17
4.7.5	X-ray Photoelectron Spectroscopy	18
4.7.6	Low Field Nuclear Magnetic Resonance	19
4.7.7	Scanning electron microscopy	19
4.7.8	Stereomicroscopy.....	20
5	MATERIALS AND METHODS.....	22
5.1	Reagents and solutions.....	22
5.2	Preparation of Composites Hydrogels	22
5.3	Swelling Study	25
5.4	Fourier Transform Infrared Spectroscopy - Attenuated Total Reflectance	25
5.5	Differential Scanning Calorimetry.....	25
5.6	X-Ray Diffraction	25
5.7	X-ray Photoelectron Spectroscopy	26
5.8	Low-Field ¹ H Nuclear Magnetic Resonance	26

5.9	Morphology Study	27
6	RESULTS AND DISCUSSION	27
6.1	Molecular Characterization and Estimated of degree of deacetylation of Chitosan -A and -I	27
6.1.1	Fourier Transform Infrared Spectroscopy	27
6.1.2	X-Ray Diffraction	30
6.1.3	Low-Field ¹ H Nuclear Magnetic Resonance.....	31
6.2	Characterization of Composite Hydrogels.....	33
6.2.1	Synthesis process and Physical characteristics	33
6.2.2	Swelling Study	35
6.2.3	X-ray Diffraction	37
6.2.4	Fourier Transform Infrared Spectroscopy - Attenuated Total Reflectance	38
6.2.5	Differential Scanning Calorimetry.....	40
6.2.6	X-ray Photoelectron Spectroscopy	41
6.2.7	Morphology Study	48
6.2.8	A Suggested Chemical Structure of the composite Hydrogels.....	50
7	CONCLUSIONS AND RECOMMENDATIONS	52
	BIBLIOGRAPHY.....	53
	ANNEXES	65
	ANNEX 1 List of reagents used.....	65
	ANNEX 2 Composites hydrogels with CH-A drying at room temperature dry state and swollen state after swelling 24 hours in 25ml of water	67

LIST OF TABLES

Table 1: Composition of the hydrogels and their potential applications ⁵⁰	11
Table 2: Composition and code of composite hydrogels dried at room temperature.	23
Table 3: FT-IR assignments for CH-A and CH-1 ^{105,106}	29
Table 4: Degree of deacetylation (DD%) of chitosan CH-A and CH-I by FT-IR and ¹ H NMR-LF related with corresponding crystalline index by XRD.....	31
Table 5: Surface elemental compositions of CH-A, CH-I, and CH A-18 Glycerol composites hydrogels.....	46
Table 6: Relative intensities of the fitted C1s peak of CH-A and CH A-18 Glycerol composites hydrogels.....	47
Table 7: Relative intensities of the fitted N 1s peak of CH-A and CH A-18 Glycerol composites hydrogels.....	47

LIST OF FIGURES

Figure 1: Composition of the first cell wall of plants ²⁸	5
Figure 2: Carboxymethylation reaction is taken from Abdulhameed ³⁴ et al.	8
Figure 3: Controlled drug release in hydrogels ⁶¹	13
Figure 4: Graphical representation of ATR infrared spectroscopy ⁷⁶	16
Figure 5: Block diagram of Heat Flux DSC taken from Stark ⁷⁹ et al.....	17
Figure 6: X-ray Photoelectron Spectroscopy ⁸⁷	18
Figure 7: Representation of the operation of the Scanning electron microscopy taken from Inkson ⁹⁷	20
Figure 8: The two main stereomicroscope optical designs: (a) CMO. (b) Greenough ⁹⁸	21
Figure 9: Composite hydrogel preparation procedure.	24
Figure 10: FTIR CH-A and CH-1	28
Figure 11: Calculation of areas in FTIR CH-A and CH-belonging to groups -CH AND -CO. ..	30
Figure 12: XRD patterns CH-A and CH-I.....	31
Figure 13: LF ¹ H NMR chitosan CH-A and CH-1.	32
Figure 14: Deconvolution LF 1H NMR chitosan CH-A and CH-I	32
Figure 15: Behavior of AC in hydrogel composites causing a more compact matrix.....	33
Figure 16: Composites hydrogels without drying and samples air-dried at room temperature...	34
Figure 17: Behavior of AC in hydrogel composites causing a more compact matrix.....	34
Figure 18: CMC/CH-A-CA24-G18 without drying and samples air-dried at room temperature	35
Figure 19: Swelling ratio of sponge hydrogels prepared with CH A and CH I at different ratio of glycerol and citric acid : (a)CH A-0 Glycerol,(b)CH A-18 Glycerol,(c) CH A-36 Glycerol, (d) CH I-0 Glycerol,(e)CH I-18 Glycerol and (f)CH I-36 Glycerol.	36
Figure 20: XRD(a)CMC,(b)CH-A and (c) CH A-18 Glycerol.....	37
Figure 21: FT-IR of composites hydrogels prepared with CH A and CH I at different ratio of glycerol and citric acid : (a)CH A-0 Glycerol,(b)CH A-18 Glycerol,(c) CH A-36 Glycerol, (d) CH I-0 Glycerol,(e)CH I-18 and (f)CH I-18.	39
Figure 22: FTIR composites hydrogels matrices at different ratios of CA, CMC, and CH A-18 Glycerol.....	40

Figure 23: DSC analysis of CMC/CH-CA48-GL18 : (a)first heating from 20 C° to 120 C°,(b)second heating of 20 C° to 200C°	41
Figure 24: Survey XPS of (a)CH-A, (b)CH-I,(c) CMC/CH-A-CA24-G18,(d)CMC/CH-A-CA36-G18,(e) CMC/CH-A-CA48-G18 and,(e) CMC/CH-A-CA96-G18.	43
Figure 25: Survey XPS of C1s spectrum CH-A and CH A-18 Glycerol composites hydrogels	44
Figure 26: Survey XPS of N1s spectrum CH-A and CH-A-18 Glycerol composites hydrogels	45
Figure 27: Stereomicrographs at x2.5 magnification of (a) CH/CMC-CA36-G18 (b) CH/CMC-CA96-G18.....	48
Figure 28: SEM micrographs of the transversal surfaces of CH A-18 Glycerol with the following magnifications(a) 2mm, (b)100um, (c)100um, and (d)10um	49
Figure 29: Reaction equation of the composites hydrogels formation..	51

1 INTRODUCTION-JUSTIFICATION:

Hydrogels, or hydrophilic gels, are structures constituted in three-dimensional networks through cross-linked, which are capable of holding considerable large amounts of water, but they do not dissolve in water. Their ability to absorb water comes from the presence of hydrophilic functional groups on the polymeric matrix (-OH, -COOH, -CONH₂, -CONH -SO₃H and NH₂), while their resistance to be dissolved originates from cross-linking of polymer chains¹. Hydrogels have a variety of natural sources and they have presented the following significant characteristics: non-human toxicity, biocompatibility, high biodegradability, retention of certain biological fluids². Hydrogels have generated growing interest in the fields of agriculture, material, environment, and biomedical applications¹.

Hydrogels have two classifications of crosslinking, chemical or physical. Chemical crosslinking is in a permanent configuration due to covalent bonds with the use of esterifying agents and high temperatures. On the other hand, physical crosslinking is in a changing configuration due to interactions of a physical nature such as: hydrogen bridges, ions, hydrophobic forces, and natural crosslinking between the different fibrils of the polymer¹.

Cellulose is ranked as the most abundant biomolecule on the planet and currently, research has increased exponentially due to its abundance and the range of possibilities it offers^{3,1}. The presence of hydroxyl groups incorporate hydrogen bridges, and that favors properties and hydrophilicity and improved mechanical resistance compared to other materials^{1,4}. Carboxy methyl cellulose, CMC, is one of the main derivatives of cellulose. Unlike cellulose, it is soluble in water, carboxymethyl groups confer negative charges on the molecule, becoming hydrophilic. It has been used in lubricating eye drops, an intimate hygiene product in addition to areas of bioengineering research^{5,6}.

Chitosan, CH, is the most important derivative that is produced from chitin present mainly in the exoskeletons of crustaceans and insects mainly. These molecules have amino groups that confer characteristics suitable for the sustained release of drugs and antimicrobial properties. Furthermore, chitosan is biocompatible and biodegradable, making the material highly desired for pharmaceutical industries, as well as tissue engineering research⁷.

Ecuador in 2019 reached an export of approximately 1,400 pounds of shrimp⁸. According to Varun⁹ *et al.* They report the possibility of converting this waste material into value-added materials such as CH in addition to chitooligomers. Iqbal¹⁰ supports the idea of processing shrimp shells to obtain chitosan with high degrees of deacetylation, using adequate amounts of HCl and NaOH. Therefore, for Ecuador, this could be an industry source for chitosan in addition to its use of biomedical applications.

Hydrogels from CMC and CH in conjunction with other wide ranges of natural or synthetic polymers have undergone chemical characterization, mechanical tests, *in vitro* and *in vivo* tests. They have shown excellent properties: mechanical, swellability, biocompatibility, biodegradability, antiseptic, scarring, morphological and thermal suitable for the use of dressings in the repair of human skin^{11,12,13,14,15}. The wide range of applications could range from burns², artificial skin¹⁶, cancer such as melanoma¹⁷, cosmetic area¹⁸, treatments for diabetics, etc¹⁹.

Previous studies have reported the synthesis of sponges based on cellulose variants, including CMC together with CH, maintaining the peculiar properties of each component, even making synergy in certain characteristics of the final materials²⁰⁻²¹.

In this work, hydrogel composites based on blends of CMC and CH were prepared at room temperature using, glycerol and acetic acid, AC, as a plasticizer and crosslinking agent respectively. The novelty of this research rest on an unconventional mixing method to achieve an adequate homogenization in the material, and in the influence of the crosslinker in the matrix of the hydrogel composites.

2 PROBLEM STATEMENT

Both CMC and CH have been studied for years for their diversity of mechanical and health properties, making them suitable materials to produce a variety of hydrogels. Currently, the demand for new materials for tissue engineering worldwide has grown, but with barriers to overcome, such as material availability, biocompatibility, and accessible costs²². Tissue engineering today is costly in some cases inefficient due to rejections produced by the body itself. For these reasons, research and development are important to find new bioengineering materials with the principles of green chemistry, equally effective and at more accessible costs.

3 GENERAL AND SPECIFIC OBJECTIVES

3.1 General objective

- Development of a green synthesis and characterization of composite hydrogels based on chitosan and carboxymethyl cellulose.

3.2 Specific objectives

- Development of a green road for synthesizing composite hydrogel.
- Study the effect of citric acid as a chemical crosslinker.
- Test glycerol as plasticizer.
- Compare the effect of polymorphs of chitosan (α and β) on the composite hydrogel final properties.
- Study of physicochemical, morphological, and thermal properties of composite hydrogels.

4 THEORETICAL BACKGROUND

4.1 Hydrogels

4.1.1 History and importance of hydrogels

In 1938 the first water adsorbent was synthesized which consisted of acrylic acid and divinylbenzene through a polymerization reaction¹. The first hydrogels were developed 12 years later by Otto Wichterle of Czechoslovak origin (1913-1998) who developed as a chemist, teacher, and inventor²³. Among his best-known inventions are contact lenses which consisted of poly (hydroxyethyl methacrylate) which reached swellings of forty to fifty percent improving the quality of life of people with eye problems. Subsequently, hydrogels began to develop for the intimate use of women, then hydrogels evolved into diaper development. In 2014, the industry of super adsorbent polymers produced approximately 2 million tons, it is expected that within two years the production will increase by 3 million tons. By 2020, the super-absorbent polymer market will be estimated at approximately \$ 8 trillion¹.

4.1.2 Hydrogels Definition

Hydrogels are composed of polymers in three-dimensional networks which have a variety of properties such as: hydrophilicity, permeability, low coefficient of friction, and high indexes of swelling. These can swell hundreds of times their dry weight because in their structure there are the presence of polar groups capable of trapping liquids, the crosslinks prevent their dissolution¹.

4.1.3 Types of hydrogels in accordance with crosslinking

The crosslinks between hydrogels are of two chemical and physical types. Chemical crosslinks are capable of covalent bonding which will dispose of the hydrogel in a permanent structure. On the other hand, physical crosslinks produce ionic interactions, molecular entanglements, and hydrophobic forces which will cause the hydrogel to change structure when faced with temperature stimuli¹.

4.1.4 Hydrogel classification according to the type of application

Hydrogels depending on their composition and unique properties have produced a variety of applications such as: controlled drug release, tissue engineering, biosensors, energy storage²⁴, dye

removal, heavy metal removal, art restoration, electrolytic solutions, anode and cathode design, agriculture among others.

4.2 Cellulose

Investigations concerning cellulose has increased dramatically because it is the most abundant biomolecule in the world and consists of D-glucose linked by B-1,4 glucosidic bonds^{24,25,26}. Cellulose is produced by bacteria or is present in plants with hemicellulose, lignin, pectin, and residual starch²⁷, Figure 1 shown the composition of cell wall and its main components. Cellulose has high indices of hydrophilicity, mechanical resistance, biodegradability, chirality, and chemical modification through hydroxyl groups for the generation of new properties¹.

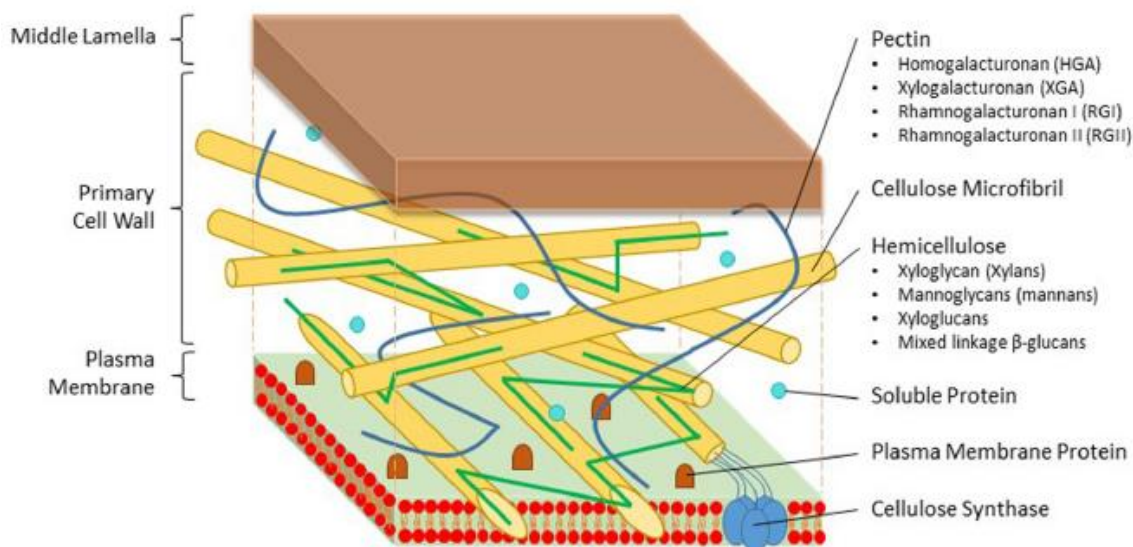


Figure 1: Composition of the first cell wall of plants²⁸

The cellulose source subjected to the different treatments affects the degree of polymerization producing amorphous and crystalline regions. The most used methods to isolate cellulose are grinding treatments, the use of Na(OH) in certain concentrations, as well as high temperatures to increase the degree of polymerization²⁷. The degrees of crystallinity reached vary between forty to seventy percent. Methods such as microwaves, ultrasound, and ammonia pretreatments have also been reported, but these do not have large-scale or industrial viability¹.

4.2.1 Cellulose polymorphisms

Depending on the orientation of the cellulose chains and hydrogen bonds, the following polymorphisms I, II, III, and IV have been determined. The native cellulose is known as cellulose I. It is in a parallel chain configuration, the conversion to cellulose II occurs through mercerization with sodium hydroxide, changing the configuration to antiparallel chains²⁶. Cellulose III can be obtained from the previous celluloses with a treatment of liquid ammonia or some amines²⁴. Polymorphs II and III can be transformed to IV using a treatment with glycerol at temperatures ranging from 200 to 260C to be finally washed with 2-propanol and water^{4,29,30}. Cellulose IV is similar to the starting celluloses in spectroscopic studies, differing only by various degrees of lateral disorder³⁰.

4.2.2 Nanocellulose

Nanocellulose (CNF) is also defined as nanofibrils that have at least one dimension on a scale of 1-100nm. This type of cellulose has chemical and physical properties such as: solubility in water, transparency, nanoporosity, large surface areas, and a high surface-volume ratio. Nano fibrils can be produced by bacteria or plants by using decay methods using mechanical forces or chemical compounds¹. For the preparation of nanocellulose, there are a variety of methods: acid hydrolysis, ultrasound, high pressure treatment, cryocrushing, grinding treatment, and enzymatic hydrolysis²⁶.

4.2.3 Crystalline nanocellulose

Crystalline nanocellulose (CNC) also known as cellulose nano crystals are produced by acid hydrolysis using sulfuric acid or hydrochloric acid to break down amorphous regions and maintain the crystalline regions improving mechanical properties. The dimensions of the nanocrystals concerning the diameter are 3-5 nm and in lengths, they have variations of 200-500 nm, although the length may have variations in micrometers these characteristics allow mechanical properties such as tensile strength of 7.5 GPa and Young's modulus of approximately 140 GPa¹.

4.2.4 Nanowhiskers

The nanowhiskers (CNW) within the hydrogels function as a reinforcing agent improving mechanical properties. Both CNF and CNW have excellent physical properties with high

resistance modules, low coefficient of thermal expansion, high thermal stability due to the degree of crystallinity. These types of cellulose are prepared by hydrolytic treatment from the cellulose source through the use of a strong acid followed by the use of machinery that produces the shearing effect²⁶. According to Araki and Miyayama²⁵, they report nanowhiskers with widths on the nanometric scale of 14 ± 4 and 25 ± 8 , lengths 212 ± 39 and 713 ± 255 respectively for cotton and tunicin.

4.3 Carboxymethyl cellulose

Carboxymethylcellulose (CMC) is an anionic molecule as its name indicates, due to the presence of carboxymethyl groups (-CH₂-COOH), it is currently one of the most widely used cellulose derivatives due to its hygroscopic nature⁴. Applications include pharmaceutical, agriculture, cosmetics, food, ceramics, construction, adhesives, and biomedical applications. In the field of wound healing, CMC has properties: biocompatibility (bones, oral membranes, and skin), absorption of exudate, antimicrobial, malleable, it promotes autolytic debridement as well as the formation of blood vessels³¹.

4.3.1 Synthesis of Carboxymethylcellulose

The carboxymethyl cellulose is produced through cellulose that swells in the presence of NaOH, in addition to the use of the organic inert solvent that can be (isopropanol, ethanol) which has a swelling and expansion function, the reaction is carried out with an etherification which can be monochloroacetic acid (MCAA) or sodium salt (Na-MCA). Hydroxyl groups are replaced by carboxymethyl groups in the following order C2, C6, and C3 according to the carboxymethylation reaction in Figure 2. Approximately 30 percent of etherifying agent will be consumed and will form predominantly by hydrolysis of chloroacetate should subsequently be neutralized and purified^{31,32,33}.

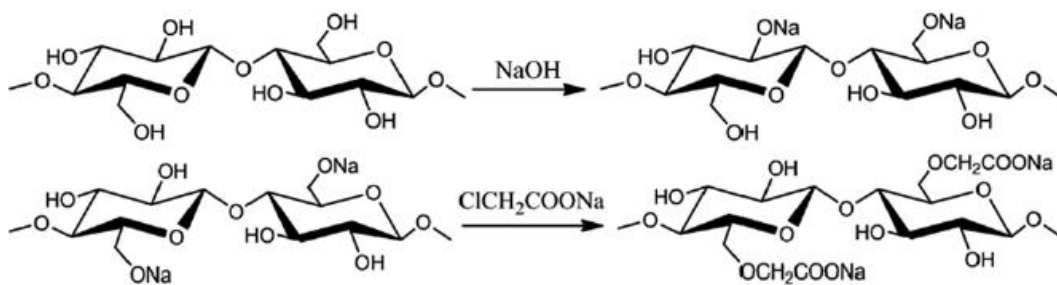


Figure 2: Carboxymethylation reaction is taken from Abdulhameed³⁴ *et al.*

4.3.2 Hydrogels based on CMC, CA, and other compounds

Mali³⁵ *et al.* synthesized carboxymethyl cellulose-tamarind hydrogel films were loaded with moxifloxacin hydrochloride and were characterized by: differential scanning calorimetry, solid state nuclear magnetic resonance spectroscopy and attenuated infrared spectroscopy of Fourier transformed total reflectance. The films were evaluated by the amount of carboxyl and the swelling index. When groups carboxyl increased in the matrix of the polymer as well as citric acid increased provoke a degree of swelling decreased. The tests demonstrated a diffusion coefficient greater than 0.5 and hemolysis tests indicate the viability of hydrogel for drug delivery. The procedure was based on previously performing the isolation of tamarind gum, it was then cross linked through esterification using a magnetic stirrer at room temperature. They were left to stand overnight to remove the air bubbles, after which they were dried at 50 degrees for 24 hours. Curing to achieve crosslinking was at 140C for 5 minutes. The films were then washed and neutralized, then the films were dried in an oven with hot air at 50C for 24 hours and stored.

Demitri³⁶ *et al.* manufactured hydrogels based on: CMCNa with HEC and as CA crosslinking agent. Initially, a concentration of two percent by weight of water in a ratio of 3 to 1 was used in the polymers dissolved in water with gentle stirring until a clear solution was obtained. First, HEC dissolves after 5 minutes, they observed that the viscosity increased, then the CMCNa was put until it becomes transparent for up to 24 h increasing the viscosity, later the concentrations at CA were varied to vary the degree of reticulation. Finally, they were allowed to dry at 308 C to remove the absorbed water and were subsequently kept at the same temperature for the crosslinking reaction. Superadsorbents within the agriculture area.

4.4 Chitosan

CH is the second most abundant polysaccharide after CMC, the molecule has amino functional groups with a positive charge, groups that can repel the structures of certain bacteria^{15,18}. Chitosan is of vital importance for a diversity of industries such as: agriculture, food, drugs, cosmetics, etc. Depending on the degree of purity or deacetylation, this material has high costs. Among the main properties of this material are: biocompatibility, biodegradable, non-toxic, antibacterial, hemostatic, anti-inflammatory, and bioresorbable^{37,38,39}. This material has a variety of biomedical applications: drug transport, tissue engineering, bone replacement, cartilage, and wound dressings^{37,40,41}.

4.4.1 Types of chitosan

Chitosan is found in the form of chitin present in the following sources: crustacean shells, insect cell walls, and fungi⁴². Chitin is transformed into chitosan through biological and chemical treatments such as hydrochloric acid and sodium hydroxide which will eliminate: acetyl groups, pigments, proteins, and calcium carbonate in turn creating a variety of chitosan with different degrees of acetylation that have a range of sixty to ninety-eight percent^{10,15,43}. According to Jampafuang⁴⁴ *et al.* There are three types of chitin polymorphisms that have been found: α consisting of an anti-parallel chain arrangement, β has a parallel configuration, and γ has a mixture of the arrangements already mentioned. Therefore, polymorphisms of chitosan leads to the presence of hydrogen bridges in α chitosan and the absence of those bridges in chitosan β .

4.4.2 Films and hydrogels of chitosan

Zhuanj⁷ *et al.* synthesized films from chitosan, glycerin, and citric acid through drying conditions at room temperature followed by heating under vacuum at 80 C for 12 hours causing amidation reactions, ionic bonds without esterification achieving excellent elastic, antibacterial properties to *Staphylococcus aureus* and *Escherichia coli*, low levels of oxygen permeability. This material could be used for the realization of membranes and food packaging.

Zheng⁴⁵ *et al.* manufactured films using chitosan, glycerol, and citric acid as crosslinking agents causing variations in water resistance. The methodology is based on reported mixtures subjected to heating of 60 C for one night and subsequently heated to 110 C for six hours and finally washed. The use of citric acid reacts with amino groups forming a cyclic amide without occurring

esterification, confirmed by infrared spectroscopy, on the other hand, glycerol provides flexibility and reduces water absorption. By increasing chitosan, it absorbs more water and the purpose of this methodology is a green technology for the formation: of packaging and drug release films.

Zhag¹⁹ *et al.* designed a hydrogel to promote wound healing through the following listed compounds: chitosan, heparin, γ -glutamic acid with the drug superoxide dismutase was prepared through a homogeneous solution where electrostatic interactions occur, ultrasound, lyophilization, and pH adjustment. The materials demonstrated good physical properties as well as an improvement in epithelial regeneration and collagen formation in rats with diabetes.

Mohandas⁴⁶ *et al.* reported injectable chitosan hydrogels loaded with arginine and nanocurcumin. The chitosan hydrogel was prepared by dissolving in acetic acid and adjusting the pH with sodium hydroxide until reaching neutral pH where the chitosan chains are grouped, later the missing components were added. The proposed hydrogel was subjected to different biological tests and proposed as a treatment for endothelial dysfunction caused by hypoxia.

4.5 Sponges based on chitosan and cellulose

Cai⁴⁷ *et al.* prepared a sponge for controlled drug release based on carboxymethylcellulose and chitosan. They tested three models gentamicin, ibuprofen, and roxithromycin, obtaining the best results for the first one, they also found that an increase in CMC and at a more basic pH leads to a better drug load, therefore better antibacterial properties. Wang²⁰ *et al.* synthesized sponges based on carboxymethyl chitosan, sodium carboxymethylcellulose, and as crosslinker γ - (2,3-epoxypropoxy) propyltrimethoxysilane. The material produced has: capillary imitation, biocompatibility, and proven high-speed hemostasis in rats. Fan⁴⁸ *et al.* elaborated a sponge from cellulose extracted from Barca wood pulp to obtain a foam gel to later be lyophilized, afterwards the samples were immersed in certain amounts of chitosan, surfactant, pore foam and again placed in lyophilization. The sponge was tested on an arterial leg wound in rats, achieving hemostasis in less than two minutes, as well as biocompatibility, becoming a promising candidate for serious bleeding¹². Cheng⁴⁹ *et al.* designed sponges for wound dressings that contain GTPMS as a crosslinker, cellulose nanofibers, and chitosan which were mixed and frozen at -50°C , later lyophilized and heated to 110°C to induce crosslinking. The materials have gas permeability, biocompatibility, absorption of exudate, blood compatibility, and hemostatic properties.

4.6 Bioengineered hydrogels

Hydrogels can be synthesized from polysaccharides or polymers of synthetic origin for the construction of frameworks with soft tissue forms such as cartilage or hard tissues such as bones. In terms of healing, the most used components for the production of hydrogels are based on: bacterial cellulose, chitosan, and collagen, since they accelerate the healing processes, Table 1 tabulates different compounds and their detailed medical applications⁵⁰. Cellulose in conjunction with other polymers is used to improve properties: mechanical, analgesic, antimicrobial, improvement of healing, and antitumor. The most used techniques for the production of fabric with defined shapes are through: molds, electrospinning, and the use of 3D printers⁵⁰.

Table 1 Composition of the hydrogels and their potential applications⁵⁰.

Hydrogel	Medical Application
PLGA	Drug delivery, Tissue engineering, cancer treatment, and imaging.
Photo-polymerizable	Tissue regeneration for bone, cartilage, and soft tissue, injectable controlled release devices for drug delivery
LNC	Drug delivery, Chemotherapeutical agent delivery(glioblastoma)
Theranostic	Drug delivery (cancer treatment), diagnostics.
TGP	Food additives, pharmaceutical, ingredients, agricultural products
Collagen	Tissue engineering, Drug delivery, cosmetic, pharmaceutic and food industry, etc.
Chitosan	Tissue engineering, drug delivery systems; wound dressing, antimicrobial agent.
Alginate	Tissue engineering, drug delivery systems.

4.6.1 Hydrogels for skin tissue engineering

The skin is known as the largest organ which performs vital functions such as: protection against bacteria or infectious agents, temperature regulation, protection against external factors such as chemicals, and physical^{51,52}.

The skin is composed of two inner layers and one outer that are epidermis, dermis, and subcutaneous tissue. The first layer serves as a barrier against the environment and this is mainly made up of cells called keratinocytes which are rich in keratin responsible for stimulating epithelial growth. The middle layer is responsible for giving strength and flexibility, it is mainly made of

collagen, elastin, and hyaluronic acid. The deepest layer is made up of fat cells, specialized collagen, and blood vessels which are in charge of storing energy and general isolation of the entire body⁵¹.

4.6.2 Hydrogels artificial skins

Capanema⁵³ *et al.* synthesized hydrogels from carboxymethyl cellulose and poly ethylene glycol through citric acid esterification reporting super absorbent hydrogels with ranges from 100 to 5000 percent. Hydrogels possess human cellular compatibility, elastic modules, non-toxicity and it is inferred that they could participate as skin substitutes and regeneration. Song⁵⁴ *et al.* manufactured a hydrogel based on nanocrystals of cellulose, borax, and polyvinyl acetate through the formation of hydrogen bonds, the hydrogel was characterized by having excellent mechanical properties for artificial skin engineering applications.

4.6.3 Hydrogels regeneration of skin tissue

Fawal⁵⁵ *et al.* manufactured a hydrogel based on hydroxyethyl cellulose with the addition of tungsten oxide IV and as a cross-linking agent to citric acid, they obtained a hydrogel with porosity and swelling properties capable of healing, in addition to presenting antibacterial properties against strains: gram-negative and gram-positive. Liu⁵⁶ *et al.* synthesized hydrogels with antibacterial and hemostatic properties through the use of cellulose nanofibrils arranged in ultrasound for the formation of the hydrogel, later the incorporation of aminated nanoparticles, and finally lyophilization. The results were a hydrogel capable of stopping bleeding, antibacterial properties, biocompatibility, and healing through tests in mice. Shefa⁵⁷ *et al.* prepared a hydrogel composed of oxidized cellulose nanofibers using the TEMPO technique, incorporating curcumin dissolved in pluronic, the hydrogels were formed using the freeze and thaw technique by forming hydrogen bonds. The hydrogels were tested in mice causing faster healing and with better results. González⁵⁸ *et al.* produced hydrogels by the freeze-thaw method using polyvinyl alcohol cellulose nanowhiskers as components, the gels proved to have a barrier against microorganisms such as bacteria, excellent mechanical properties capable of accelerating the healing process and could be used as a dressing for the treatment of wounds.

4.6.4 Hydrogels with modulated release of drugs for skin

Koneru⁵⁹ *et al.* produced hydrogel films from two types of sodium carboxymethyl cellulose, hydroxypropyl methyl cellulose with the incorporation of grapefruit seed extract cross-linked by esterification by the presence of citric acid, the compound demonstrated antimicrobial properties, improved elongation at break and the hydrogel could be used for the controlled release of drugs. There are also hydrogels with the ability to combat melanoma such as the use of carboxymethyl cellulose with doxorubicin crosslinked by using a citric acid crosslinking agent, through in vitro tests, the properties of modulation of the release of drugs, apoptosis of cancer cells, and decreased toxicity for normal cells¹⁷. Rakhshaei⁶⁰ *et al.* prepared a hydrogel in the form of a dressing using carboxymethyl cellulose, silica mesoporous, zinc oxide nanoparticles, and tetracycline as the main materials. undergoing sonication. The hydrogel demonstrated properties of cytocompatibility, gas permeability, and controlled drug release. The dressing could serve as a bandage with a healing function. Hydrogels can release drugs through changes in pH, temperature in Figure 3.

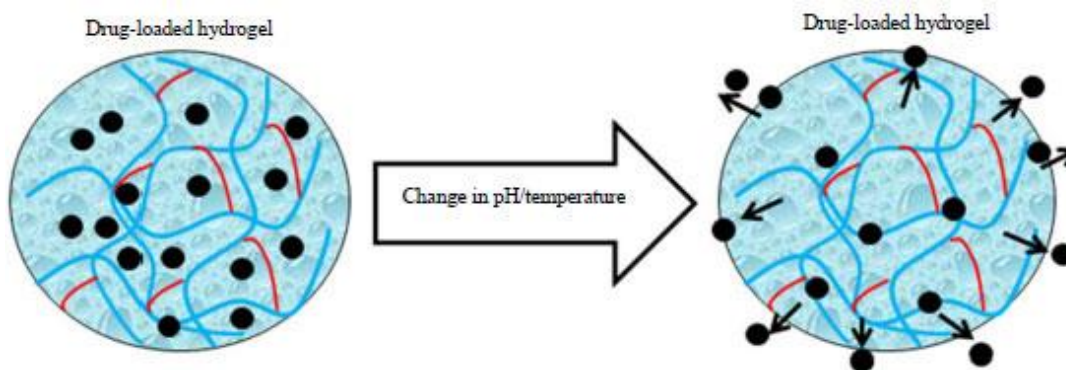


Figure 3: Controlled drug release in hydrogels⁶¹

4.6.5 Hydrogels for bone and cartilage replacement

Bones have different functions but among the main ones are: structure, protection of internal organs, calcium and phosphorus deposit, locomotion, an adequate environment for the bone marrow and it harbors specific cells that are responsible for generating blood components⁶². The structure of the bone is made up of a hard part that provides stability called osteon, a spongy part with an excellent surface area responsible for: dispersing nutrients, interacting with hormones and cytosines related to the growth and cell maintenance of bones⁶³. As a covering, the bone is

composed of the periosteum responsible for attaching ligaments, cells for regeneration, and as a complement to the blood supply⁶⁴.

Cartilage is a connective and elastic tissue with joint lining functionalities that facilitate movement, impacts, coating, and protect the joints from wear and tear. Cartilage is mainly composed of: proteoglycans, type 2 collagen, and cells called chondrocytes which are responsible for maintaining the structures⁶⁵.

At present there is an increase towards the use of polymers to replace cancellous bone tissues due to the fact that they are similar in structure, biocompatible, regenerate tissues, mechanical forces among the most used polymers are: chitosan, sodium alginate, and gelatin^{66,67}. According to Wei⁶⁸ *et al.* there are millions of people with degenerative cartilage diseases such as osteoarthritis and they summarize in a list the following components of hydrogels for replacement of cartilage matrices: chitosan, alginate, cellulose, chitosan, hyaluronic acid, fibrins, polyethylene glycol, poly (n-vinyl caprolactam) and etc⁶⁹.

Zou⁷⁰ *et al.* synthesized an oppositely charged hydrogel based on alginate and chitosan loaded with: nano-scale hydroxyapatite, bone marrow stem cells obtained from mice, parathyroid hormone, and peptides. The pores were analyzed by SEM and the structure by rheological techniques. They were verified by in vivo tests in mice that the hydrogel has biocompatibility in addition to promoting regeneration and is proposed by research for areas of tissue engineering.

Maharjan⁷¹ *et al.* manufactured a hydrogel composed of cellulose regenerated by electrospinning and chitosan using freezing techniques, improving physical characteristics. Biological tests showed that the scaffold favors the proliferation and attachment of osteoblast precursor cells.

Ghorbani⁷² *et al.* created an injectable hydrogel based on cellulose, pectin, and chitosan nanocrystals covalently crosslinked by modifications with aldehyde groups using a double cylinder needle. The hydrogel physically and biologically resembles the extracellular matrix, allowing the proliferation of chondrocytes, therefore it could be used as a treatment for cartilage regeneration.

4.7 Characterization Techniques

The characterization and determination of hydrogel network parameters offers key information when designing hydrogels with a specific structure and performance. In this section, we will present an overview of the physicochemical, morphological, and thermal characterization techniques used in this study to describe the structure of hydrogels obtained.

4.7.1 Swelling Ratio

The method consists of the immersion of dried hydrogel in distilled water at room temperature in order for it to swell. It is then taken out periodically, the excess water is removed from its surface using a filter paper, and the hydrogel is weighted. This procedure is repeated until the weight stops increasing. The swelling ratio (SR) percent is calculated according to the following equation:

$$SR(\%) = \left(\frac{Wt - Wd}{Wd} \right) 100 \quad (1)$$

Where Wt is the weight of the swollen hydrogel at time t and Wd is the weight of the dry hydrogel. The results are used to create a time vs. swelling graph that represents the kinetic behavior of the hydrogel⁷³.

4.7.2 Fourier Transform Infrared Spectroscopy-Attenuated Total Reflectance

Infrared spectroscopy is a technique widely used in the identification of organic materials' chemical structure. Infrared radiation with a frequency ranging between 4000-400 cm^{-1} offers the most practical use for the characterization of organic materials. This technique yields information on the atoms involved, their chemical bonds, and the local chemical environment within the material by measuring the vibrational transitions⁷⁴. The basic premise of this technique is the observation of radiation absorption due to the change in dipole during vibration, depending on the nature of the bond doing the absorbing we will observe a characteristic vibrational frequency. FTIR spectroscopy irradiates a sample with many frequencies of IR light at once, utilizing Michelson interferometer and using a Fourier transform to obtain the full spectrum as a function of wavenumber.

Attenuated total reflection (ATR) is a technique based on the use of an optically dense crystal with a high refractive index Figure 4. shows a graphical representation of the functioning of an ATR accessory. When an infrared beam enters the crystal at a precise angle, it is totally internally reflected creating an evanescent wave. The sample, that is pressed against the crystal, comes into contact with the evanescent wave. Depending on the frequency some waves are absorbed by the sample and become attenuated. The attenuated waves then reach the detector and the system generates an infrared spectrum⁷⁵.

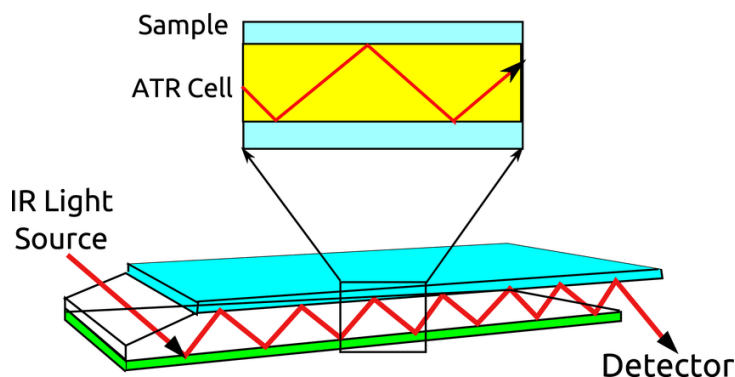


Figure 4: Graphical representation of ATR infrared spectroscopy⁷⁶.

4.7.3 Differential Scanning Calorimetry

Differential scanning calorimetry (DSC) is a technique that detects a materials' phase transitions through the change in its heat capacity with temperature. In a heat flux DSC Figure 5, a known mass of sample material and a reference are placed on a thermoelectric disk (thermal resistor) inside a temperature controlled chamber. The chamber is heated at a linear rate, and the heat is transferred to both the sample and reference through a thermal resistor. The specific heat capacity of the sample and reference create a difference in temperature that is measured by a pair of thermocouples. The resulting heat flow can be determined by Ohm's law:

$$q = \frac{\Delta T}{R}$$

Where q is "sample heat flow", ΔT is "temperature difference between sample and reference", and R is "resistance of thermal resistor"^{77,78}.

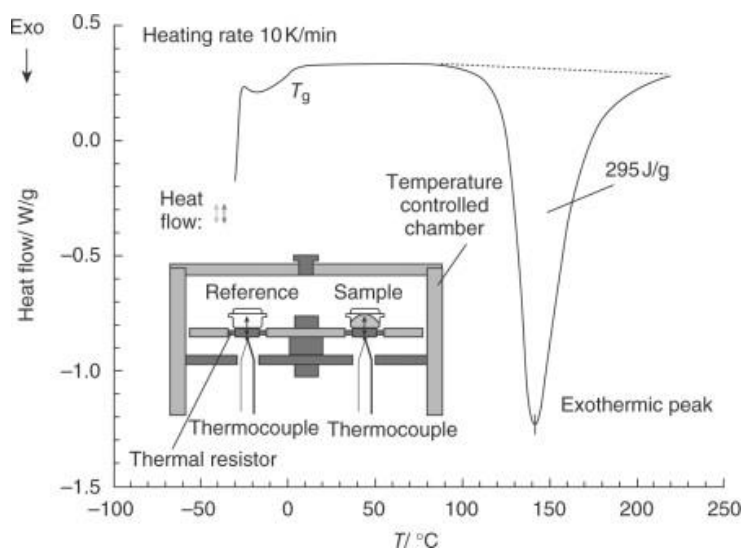


Figure 5: Block diagram of Heat Flux DSC taken from Stark⁷⁹ et al.

This technique allows knowing properties such as: glass transition temperature (T_g), specific heat capacity (C_p), thermal stability, purity, crystallization, melting, and curing^{80,78}. In the case of hydrogels, three bonding states of water molecules can be detected by DSC. Water attached directly to a polymer's hydrophilic groups through hydrogen bonding shows no phase transition from 320 to 170 K, this is denominated **nonfreezing water**. Water molecules that have a weak interaction with the polymer chain have a phase transition temperature lower than that of **free water** (bulk water) and are known as **freezing bound water**⁷⁹. The analysis of these states of water in hydrogels offers important information on their diffusion, absorption, and permeation capacities, as well as on the structure of water filled pores⁸¹.

4.7.4 X-Ray Diffraction

When light is scattered by a periodic array a constructive interference is produced at specific angles, this phenomenon is called diffraction. In a crystal, atoms are arranged in a periodic array so they can diffract light. X-Ray wavelength ranges from 1×10^{-12} - 1×10^{-10} m being similar to the distance between crystal's atoms. Therefore, the diffraction pattern produced by the scattering of X-Rays from atoms in a crystal contains information about its atomic arrangement. On the other hand, amorphous materials do not have a periodic array with long-range order, so they do not produce a diffraction pattern.

Most polymers are amorphous in character, but in the case of hydrogels, since freezing and thawing methods of preparation are used, semi-crystalline regions are produced⁸². From the X-Ray

Diffraction (XRD) technique and using the Bragg's law, we can obtain the following information about our material: percentage of crystallinity, structural composition, orientations, deformations in the hybrid hydrogel matrix, and interplanar atomic spacing¹.

4.7.5 X-ray Photoelectron Spectroscopy

X-ray photoelectron spectroscopy (XPS) or electron spectroscopy for chemical analysis (ESCA), is a surface analytical technique used for elemental characterization of surfaces at depth of 2-5 nm. Figure 6 shows a schematic of XPS equipment and typical spectra. In XPS, X-ray radiation ($Mg K\alpha$ or $Al K\alpha$), is used to irradiate a solid surface to excite the innermost levels of the atoms. Photoelectrons are emitted as a consequence of this excitation, and through the measurement of the electron kinetic energies, it is possible to obtain their binding energies^{83,84}. A photoelectron spectrum, expressed as binding energy vs relative intensity, is obtained by counting ejected electrons over a range of kinetic energies. Peaks appear in the spectrum, and their position, corresponding shapes, and intensity provide information about the molecular structure, composition, and quantity of all surface elements in the solid material^{85,86}.

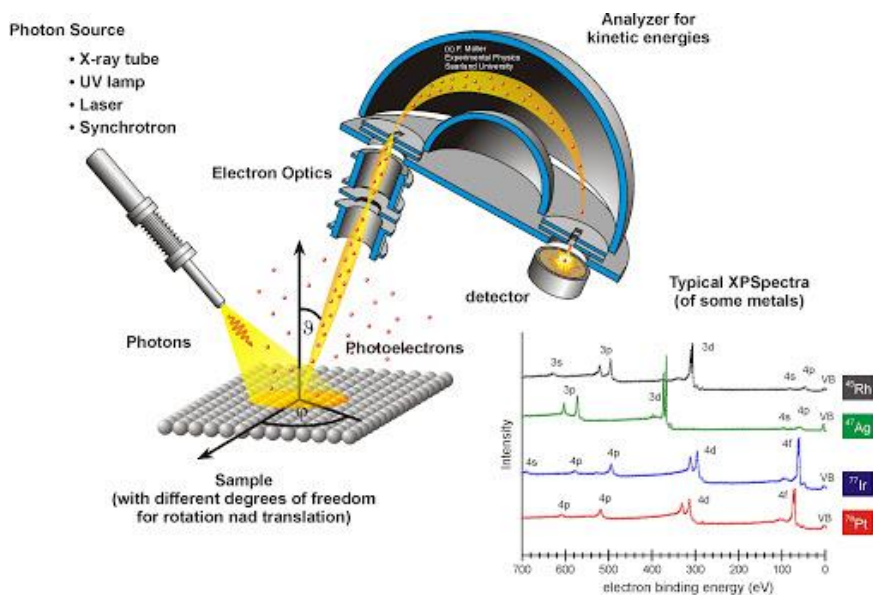


Figure 6: X-ray Photoelectron Spectroscopy⁸⁷.

4.7.6 Low Field Nuclear Magnetic Resonance

Nuclear magnetic resonance (NMR) is an analytical technique universally used in chemistry research, and industry. By irradiating atomic nuclei in magnetic fields with radio waves it can determine the chemical and physical structure of molecules^{88,89}. NMR has relatively low signal strength when compared to other spectroscopic techniques. However, this is compensated by an enormous ability to measure a wide set of molecular properties and by the ease of designing and conducting new experiments. To improve the quality of the signal in NMR the strength of the magnetic field where the sample is placed is increased, since the amplitude of the signal depends strongly on the strength of the magnetic field⁹⁰.

Although the first magnets used for NMR detection in condensed matter were electromagnets and permanent magnets, the development of superconducting magnet technology made the former obsolete. On the other hand, research and applications have not become obsolete and have had a new momentum thanks to the development of tabletop and portable instruments and new and advanced detection methods. Currently, NMR at 90 MHz ¹H resonance frequency and below is known as **lower field NMR**. There are applications in which lower magnetic fields can be advantageous, such as: foodstuffs quality control, moisture, in wood, oil painting detection, oil well logging, rock core porosity analysis, underground water detection, among others⁹¹.

Polymer molecular characterization could be performed using ¹H NMR Spectroscopy. Due to the high cost, high field NMR spectroscopy is rarely used for routine materials verification. On the other hand, low-field benchtop NMR spectrometers have been introduced commercially as a less expensive alternative. New and interesting applications have been developed to obtain information on biopolymers, among them it is worth noting the determination of the degree of deacetylation of chitosan⁹².

4.7.7 Scanning electron microscopy

The scanning electron microscopy (SEM) technique is based on the use of a tightly focused beam of high energy electrons, instead of a beam of light, in order to generate an image of the surface of solid samples, with a resolution of 50-100 nanometers^{93,94}. The electrons are accelerated through an electric field and focused with the use of specialized lenses called: condenser and objective⁹³, as shown in Figure 7. Accelerated electrons carry considerable kinetic energy, which is dissipated

during electron-sample interaction producing secondary electrons, backscattered electrons, diffracted backscattered electrons, photons (x-ray), visible light, and heat. The sample image can be formed by secondary and backscattered electrons. The first kind of electrons are used for showing morphology and topography on samples, while the second are used for rapid phase discrimination. SEM is a nondestructive technique that generates high-resolution images of shapes of objects (SEI) and acquiring maps of the variation in elemental chemical compositions by energy-dispersive x-ray spectroscopy (EDS) ^{95,96}.

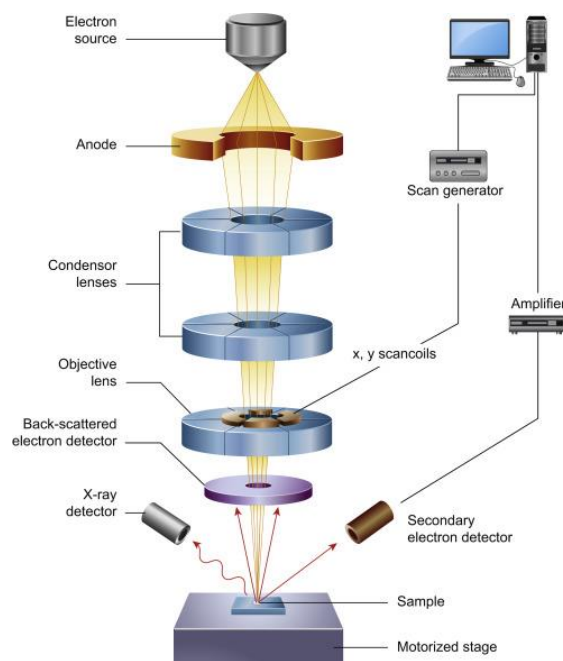


Figure 7: Representation of the operation of the Scanning electron microscopy taken from Inkson⁹⁷.

4.7.8 Stereomicroscopy

Stereomicroscopy is a technique based on the use of a microscope equipped for stereoscopic viewing with the purpose of obtaining an amplified 3D image of a sample. Stereomicroscopes have two main designs: Common main objective (CMO) and Greenough Figure 8. Greenough stereomicroscopes are typically used in industrial settings while CMO stereomicroscopes are generally utilized in research for their high resolution, advanced optical setup, and illumination accessories.

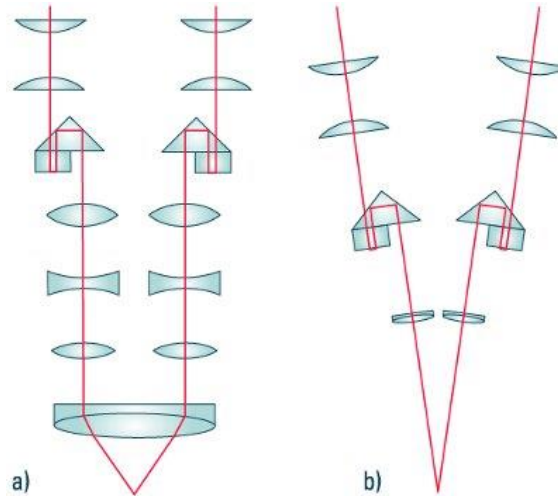


Figure 8: The two main stereomicroscope optical designs: (a) CMO. (b) Greenough⁹⁸.

The design of a CMO stereomicroscope is centered on the refraction of light by a single objective lens of large diameter through which the right and left ocular channels view the sample. Each ocular channel consists of an independent optical setup parallel from one another, this arrangement guarantees that convergence of the left and right optical axes coincides with the focal point in the sample plane. One of the major advantages of CMO systems is the absence of a tilt in the image at the eyepiece focal plane given that the optical axis of the objective is perpendicular to the sample plane⁹⁹.

5 MATERIALS AND METHODS

5.1 Reagents and solutions

- **Reagents**

Carboxymethyl cellulose sodium salt cellulose (CMC, High Viscosity grade, Loba Chemie, sodium glycolate Max 0.4%, Viscosity (2% in water, 20 °C) 1100-1900 cps). Chitosan food grade (BioFitnest) identified as CH-A and chitosan food grade (Guo Zhen international., LTD, viscosity 60-100 cps, >90% DD) as CH-I. Glycerol (GL; Molecular biology, Sigma Aldrich) and (PEG; Synthesis, Loba Chemie) was used as a plasticizer. Citric acid (CA; AR grade, Loba Chemie) was used as a chemical cross linker. Acetic acid (AA; synthesis, MM Reprintaciones) as a chitosan co-solvent.

- **Solutions**

Chitosan 2% (w / v) dissolved in 2% (v / v) acetic acid reached a (pH 5-6), CMC 2% (w / v) dissolved in distilled water reached a (pH 7), citric acid 2% (w /v), and glycerol at 10 % (v /v). All stock solutions were individually mixed for a period of 3 hours and subsequently stored in flasks.

5.2 Preparation of Composites Hydrogels

The composites hydrogels were synthesized using a CMC/CH volume ratio of 3:1 while varying the concentrations of citric acid and glycerol. Figure 9 shows the procedure followed to prepare each hydrogel composite. First, the solution of CMC was stirred for a period of 3 minutes. Then, the chitosan solution was added and mixed until reaching a homogeneous-appearing solution. To the resulting mixture CA and glycerol were added, one after the other, under stirring. All mixtures were prepared using an immersion mixer and afterwards sonicated at 40 °C for a period of 99 minutes to produce crosslinking conditions. The excess liquid was removed from each sample and dried at room temperature for one week. **Table 2** lists prepared composites hydrogels, their composition, and code name.

Hydrogel composition			Code Name	
CMC:CH (mL)	CA (mL)	GL (mL)	CH-A	CH- I
90:30	24	-	CMC/CH-A-CA24-G0	CMC/CH-I-CA24-G0
90:30	36	-	CMC/CH-A-CA36-G0	CMC/CH-I-CA36-G0
90:30	48	-	CMC/CH-A-CA48-G0	CMC/CH-I-CA48-G0
90:30	96	-	CMC/CH-A-CA96-G0	CMC/CH-I-CA96-G0
90:30	24	18	CMC/CH-A-CA24-G18	CMC/CH-I-CA24-G18
90:30	36	18	CMC/CH-A-CA36-G18	CMC/CH-I-CA36-G18
90:30	48	18	CMC/CH-A-CA48-G18	CMC/CH-I-CA48-G18
90:30	96	18	CMC/CH-A-CA96-G18	CMC/CH-I-CA96-G18
90:30	24	36	CMC/CH-A-CA24-G36	CMC/CH-I-CA24-G36
90:30	36	36	CMC/CH-A-CA36-G36	CMC/CH-I-CA36-G36
90:30	48	36	CMC/CH-A-CA48-G36	CMC/CH-I-CA48-G36
90:30	96	36	CMC/CH-A-CA96-G36	CMC/CH-I-CA96-G36

Table 2: Composition and code of composite hydrogels dried at room temperature.

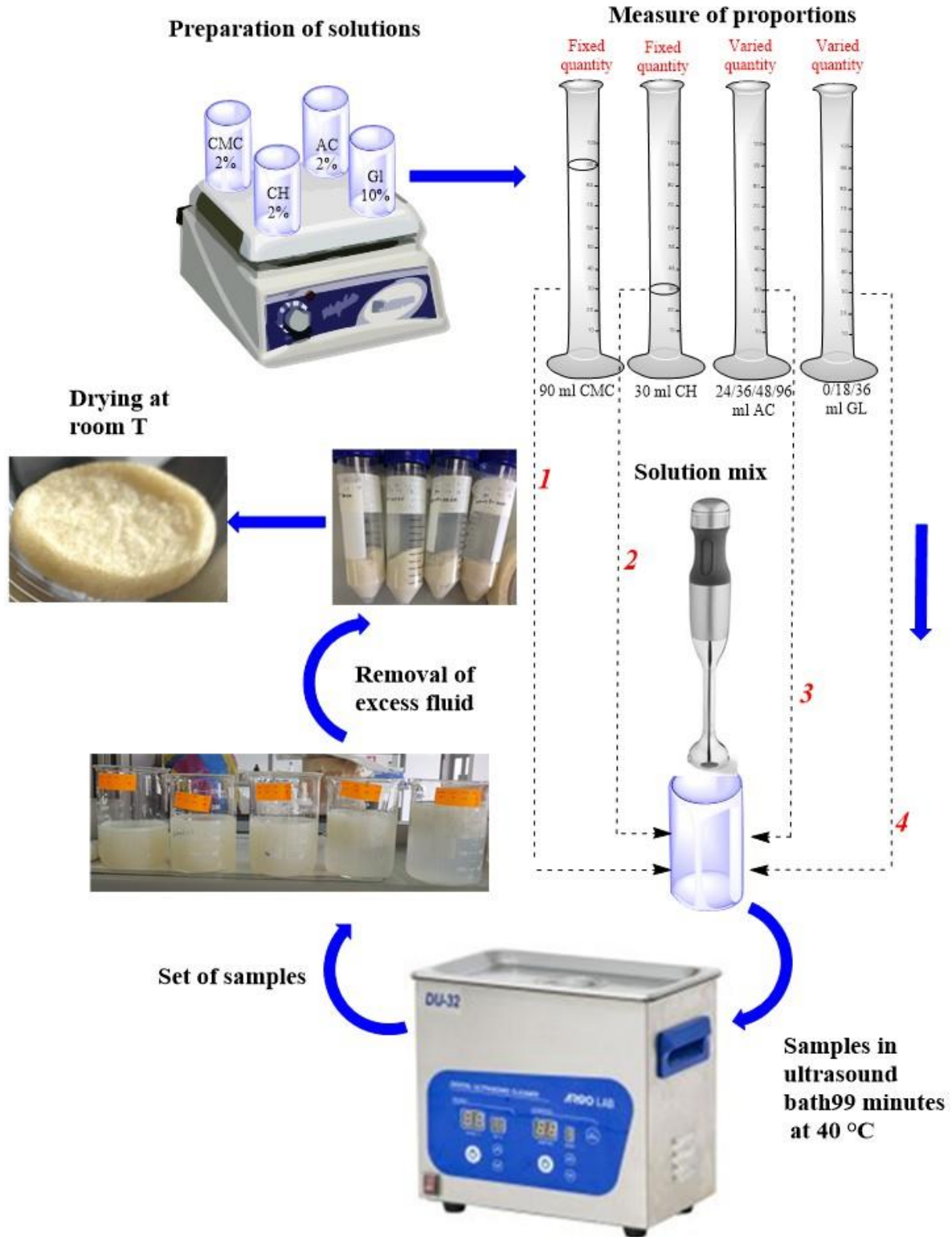


Figure 9: Composite hydrogel preparation procedure.

5.3 Swelling Study

The swelling of the composite hydrogels obtained were studied using the swelling ratio technique described in Section 4.7.1. Dried hydrogels were immersed in 30mL of distilled water at room temperature and weighted every hour for the first 5h and then every 24h till the 72h mark. The excess water was gently removed with a filter paper for weighing each time. The data obtained was then used in a time vs swelling graph.

5.4 Fourier Transform Infrared Spectroscopy - Attenuated Total Reflectance

The functional groups of CH-A, CH-I, and composites hydrogels were studied by FTIR using a Cary 630 with 1-Bounce Diamond ATR accessory. The spectra were obtained in the range of 4000–400 cm⁻¹, with a spectra resolution of 4 cm⁻¹ and 32 scans.

The composition and degree of deacetylation (*DD%*) were determined for the chitosan CH-A using CH-I as a reference. Weißpflog¹⁰⁰*et al.* methodology was used to calculate the *DD%* in accordance with the equation:

$$DD_{FTIR} \% = 100 - \frac{\left(\frac{A_{v(C-O)}}{A_{v(C-H)}}\right) \times 100\%}{1.33} \quad (2)$$

Where $A_{v(C-O)}$ and $A_{v(C-H)}$ corresponds to the areas of the stretching vibration signal of C=O and C-H, respectively.

5.5 Differential Scanning Calorimetry

Thermal Properties of a CMC/CH-A-CA36-G18 sample was studied by DSC. Perkin Elmer DSC 8000 was used to analysis the glass transition (*T_g*) property of hydrogel composites. Nitrogen was employed as the purge gas. The temperature range used was between 20-200 °C with a heating rate of 10 °C / min. The defined thermal cycle was: heating 20-120 °C; 120 °C isotherm for 3 minutes; cooling 120-20 °C; 20-200 °C heating; isotherm at 200 °C and cooling to room temperature.

5.6 X-Ray Diffraction

The crystalline structure of CH-A, CH-I, CMC, and a certain group of composites hydrogels were studied by X-ray powder diffraction. A Mini-flex-600 from Rigaku, with a D/tex Ultra 2 detector

was used. The X-Ray generator, Ni-filtered Cu K α radiation ($\lambda = 0.15418$ nm), was fixed at 40 kV, 15 mA. For collecting data, powder samples were placed on a glass sample holder, the selected angular region was $2\theta = 5^\circ$ - 90° with a step width of 0.01° .

Determination of the Crystallinity index ($CI\%$) were calculated with the method proposed by Foher¹⁰¹ *et al.* according to the following equation:

$$CI(\%) = \left[\frac{I_{110} - I_{am}}{I_{110}} \right] \times 100 \quad (3)$$

Where I_{110} ($2\theta \approx 20^\circ$) is the maximum intensity located in (110) peak and I_{am} ($2\theta = 16^\circ$) is the amorphous diffraction, arbitrary units can be used in the equation, in this case, normalized units were used.

5.7 X-ray Photoelectron Spectroscopy

X-ray photoelectron spectroscopy (XPS) analysis was performed to get chemical information on some selected CMC/CH composites hydrogels. A PHI 5000 Probe III Scanning XPS Microprobe from Ulvac phi, inc. For the sample preparation, each sample was placed onto a polymeric-based adhesive tape that was hold in a metallic mesh. High resolution deconvolution was performed using Tougaard background subtractions, and Voigtian and Gaussian functions. The software used for this purpose was Fityk¹⁰².

5.8 Low-Field ^1H Nuclear Magnetic Resonance

Low-Field ^1H Nuclear Magnetic Resonance (LF ^1H NMR) analysis was performed in order to validate the composition of CH-A and its degree of deacetylation ($DD\%$), using CH-I as a reference. LF ^1H NMR spectra were acquired on an NMReady-60e - Benchtop NMR Spectrometer– Nanalysis. The samples were dissolved in D_2O acidified with hydrochloric acid to $\text{pH} \sim 4$. The experiments were run at 32°C using a 5 mm probe. For the determination of $DD\%$ a single pulse sequence, with 16834 scans and a recycle time of 8 s between each transient was used, this allows for complete relaxation before each pulse application¹⁰³.

Hirai⁹² *et al.* method was used to calculate the $DD\%$. According with the following equation:

$$DD(\%) = \left[1 - \left(\frac{\frac{A_{H-Ac}}{3}}{\frac{A_{H2-H6}}{6}} \right) \right] \times 100 \quad (4)$$

Where A_{H2-H6} is the signal area associated to protons H2, H3, H4, H5, H6, H6' of both monomers and the A_{H-Ac} corresponds to the signal area of the acetyl group.

5.9 Morphology Study

A morphology study of dried composites hydrogel was carried out in a SZX16 stereomicroscope (Olimpus) and Phenom ProX desktop scanning electron microscope (SEM-EDS), working with an acceleration voltage of 10 KV.

6 RESULTS AND DISCUSSION

6.1 Molecular Characterization and Estimated of degree of deacetylation of Chitosan -A and -I

Due to a lack of knowledge of CH-A chemical composition, FTIR-ATR, LF ^1H NMR, and its XRD analysis were performed. Additionally, is $DD\%$ was determined by FTIR and ^1H NMR using CH-I as a reference.

6.1.1 Fourier Transform Infrared Spectroscopy

The FTIR spectra of CH-A and CH-I, are shown in Figure 10 and a detailed assignment thereof in Table 3 ¹⁰⁴. Both spectra were similar to each other, showing the characteristic bands of the chitosan. The widest band present at 3000-3600 cm^{-1} range, is associated with N-H stretching vibrations of free amino groups and O-H stretching vibrations, its widening can be explained as a result of vibrations of water and hydroxyls as well as intramolecular hydrogen bonds. C-H asymmetric stretching from $-\text{CH}_2$ groups and $-\text{CH}_3$ groups are found at 2919 cm^{-1} , and 2862 cm^{-1} respectively. C=O stretching vibrations of acetylated amino groups (amide I) appear at 1651 and 1640 cm^{-1} . The chitosan amide II band was resolved in two bands at 1584 and 1565 cm^{-1} , using a second-derivative procedure. The first is associated with vibration bending N-H of free amino groups and the second with bending N-H and stretching CN of the acetamide groups. C-H (CH_2)

symmetric bending of methylene groups and a C-H (CH_3) asymmetric bending of methyl in NHCOCH_3 group are found at 1462 cm^{-1} and 1419 cm^{-1} , respectively. The band at 1375 cm^{-1} is related to bending vibrations symmetric of methyl groups. The 1319 cm^{-1} band corresponds to C-N (amide III) stretching vibrations and N-H stretching of N-acetyl-glucosamine. C-N stretching vibrations of free amino groups appears at 1261 cm^{-1} . The band at 1149 cm^{-1} vibrations stretching asymmetric C-O-C belongs to the β -glycosidic link. Bands 1059 , 1024 , and 987 cm^{-1} correspond to C-O stretching vibration of the ring saccharide structure, and the band at 892 cm^{-1} is associated with a C-H bending of β -linked glycosidic bond^{105,106}.

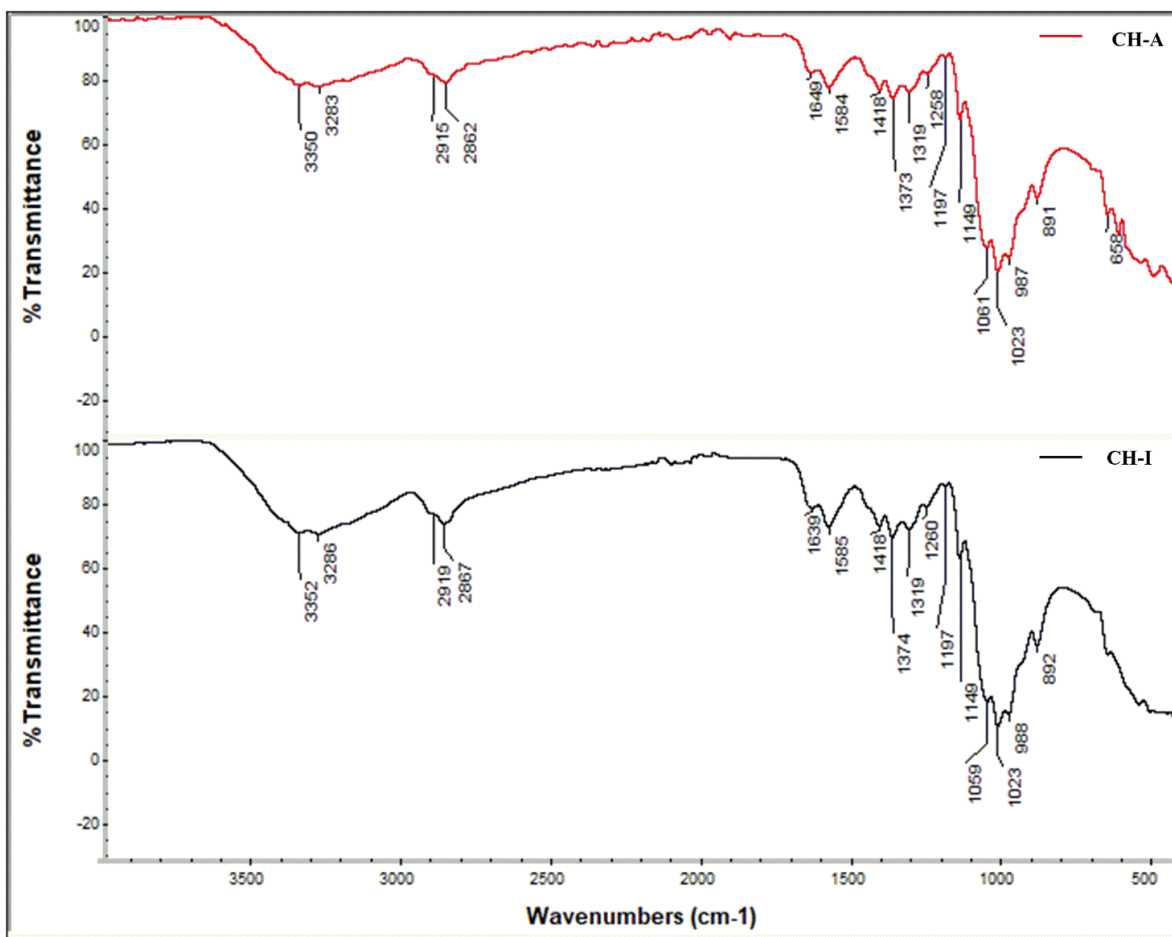


Figure 10: FTIR CH-A and CH-I .

Wavenumber (cm ⁻¹)	Vibration type	Assignments
3600-3000	ν O-H, ν N-H	N-H stretching vibrations of free amino groups O-H stretching vibrations of water and hydroxyls as well as – intramolecular hydrogen bonds
2919	ν_{as} C-H	CH ₂ in CH ₂ OH group
2862	ν_s C-H	CH ₃ in NHCOCH ₃ group
1651, 1640	ν C=O	acetylated amino groups (Amide I)
1584	δ_{ip} N-H	free amino groups
1565	δ N-H ν C-N	N-acetylgroup (Amide II)
1462, 1419	δ_s C-H (CH ₂) δ_{as} C-H (CH ₃)	CH ₂ in CH ₂ OH group CH ₃ in NHCOCH ₃ group
1375	δ_s C-H (CH ₃)	Bending vibrations of methyl in NHCOCH ₃ group
1319	ν C-N ν N-H	C–N (amide III) and N-H stretching of N-acetyl–glucosamine
1261	ν C-N	Free amino groups
1149	ν_{as} (C–O–C)	β -glycosidic link C-O-C (bridge)
1059	ν (C–O)	C–O ring saccharide structure
1023	ν (C–O)	C–O ring saccharide structure
987	ν (C–O)	C–O ring saccharide structure
892	δ C-H	β -linked glycosidic bond

Table 3 FT-IR assignments for CH-A and CH-I^{105,106}.

FTIR spectra of CH-A and CH-I are shown in Figure 11. Probe ($A_{\nu(C-O)}$) and reference ($A_{\nu(C-H)}$) bands and its corresponding baselines can be seen in this Figure 11. The degree of deacetylation was calculated using equation 2, following the methodology proposed by Weißpflug¹⁰⁰ *et al.* DD% values obtained were 90.6 and 91.8 for CH-A and CH-I respectively, and they are tabulated in the Table 4.

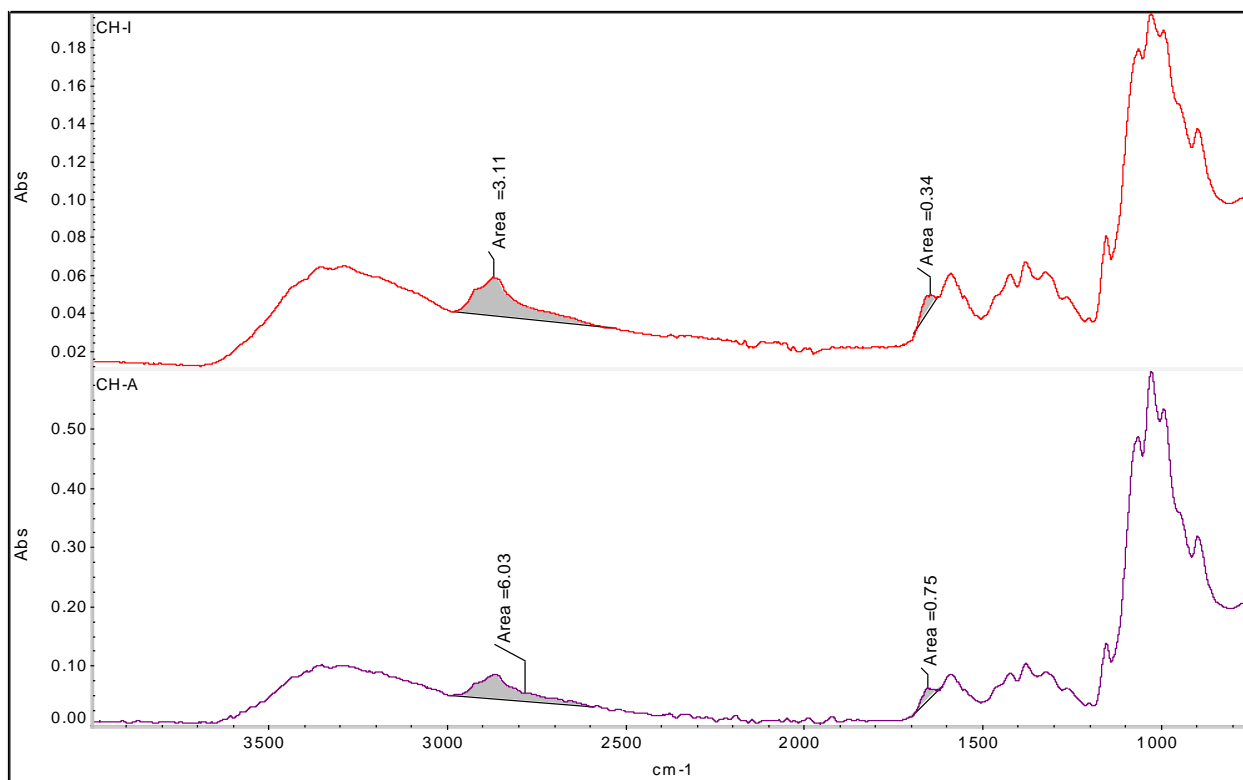


Figure 11: Calculation of areas in FTIR CH-A and CH-I belonging to groups -CH AND -CO.

6.1.2 X-Ray Diffraction

The X-ray diffraction pattern of chitosan CH-A and CH-I are illustrated in Figure 12. The XRD patterns of CH-A exhibit two crystalline peaks at $2\theta \approx 10.8^\circ$ and $2\theta \approx 20.0^\circ$ due to X-ray diffraction from the (020) and (110) planes of the semicrystalline α -chitosan powder, respectively. Additionally, a shoulder at $2\theta \approx 21.8^\circ$ can be observed. The intensity of this signal is related to $DD\%$ —an increase of intensity indicating an increment in $DD\%$ ¹⁰⁰. Furthermore, the disappearance of the intensity in the (020) plane is due to the absence of intermolecular forces related to hydrogen bridges, therefore, the CH-I corresponds to a β polymorphism and CH-A corresponds to a α polymorphism⁴⁴. Both diffraction patterns, shown a small signal at $2\theta \approx 29.5^\circ$ associated to calcite and calcium phosphate¹⁰⁷. $CI\%$ values 66.3 y 51.2 for CH-A and CH-I respectively, were obtained using equation 3, and are displayed in Table 4.

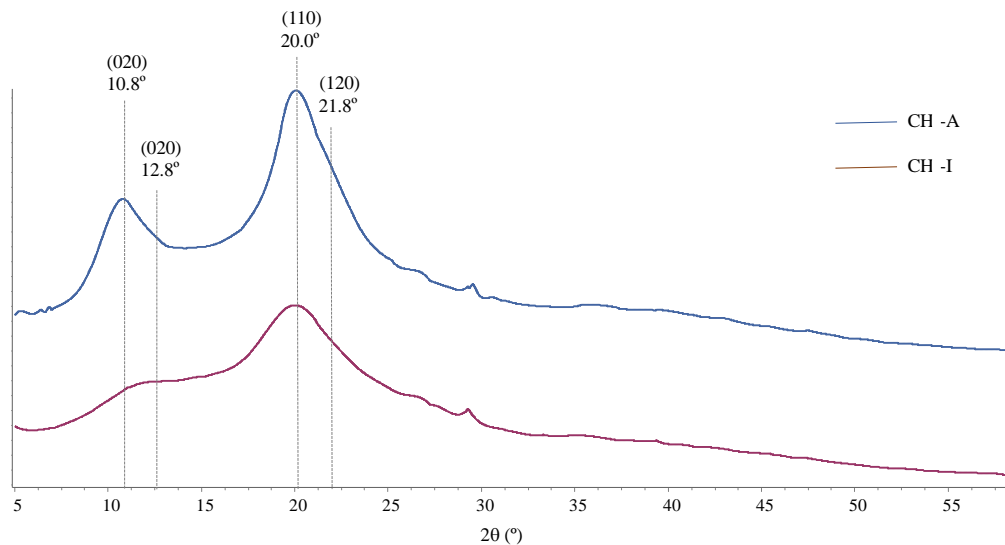


Figure 12: XRD patterns CH-A and CH-I

6.1.3 Low-Field ^1H Nuclear Magnetic Resonance

The LF ^1H NMR spectra of CH-A and CH-I were similar to each other, show the characteristic signals of the chitosan. The only differences observed correspond to changes in the relative intensities of the signals. As an example, Figure 13 shows the spectrum of CH-A together with a detailed assignment thereof ¹⁰⁸.

Signals in the spectra are overlapped, obeying to the low field and sample's high viscosities. To obtain more accurate results of the *DD%* the spectra were deconvoluted, as shown in Figure 14. *DD%* values 90.5 y 94.0 for CH-A and CH-I respectively, were obtained using equation 4, and are displayed in Table 4.

Sample	<i>DD%</i>			<i>CI</i> (%)
	FT-IR	^1H NMR-LF	specification	XRD
CH-A	90.6	90.5	-	66.3
CH-I	91.8	94.0	>90% (94.6%)	51.2

Table 4 Degree of deacetylation (*DD%*) of chitosan CH-A and CH-I by FT-IR and ^1H NMR-LF related with corresponding crystalline index by XRD.

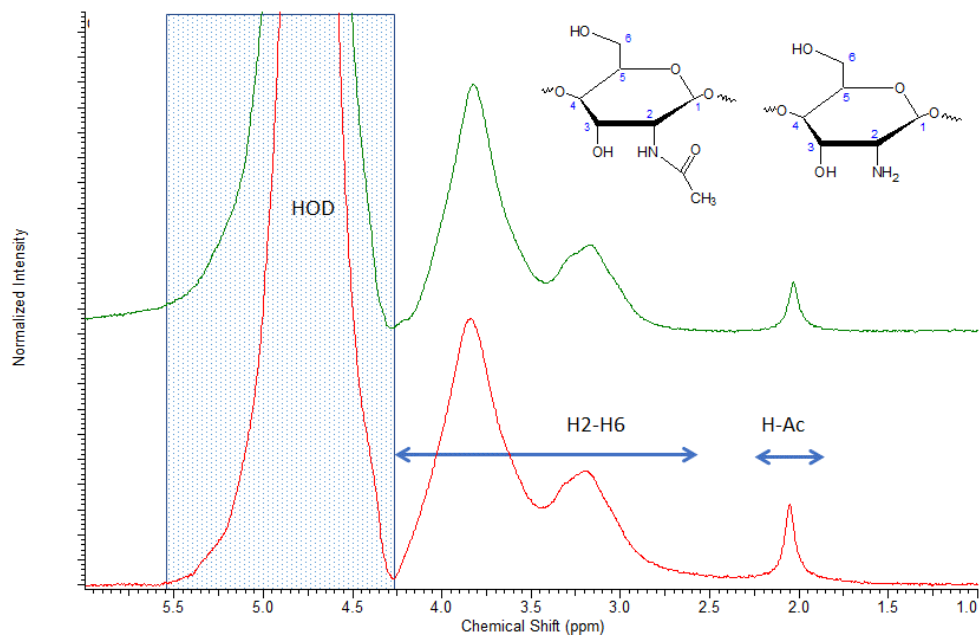


Figure 13: LF ^1H NMR chitosan CH-A and CH-I.

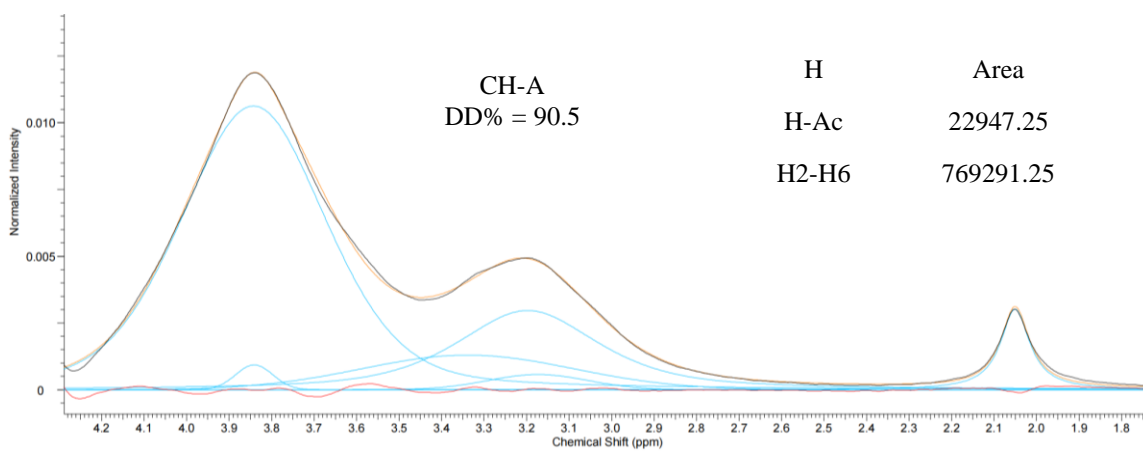
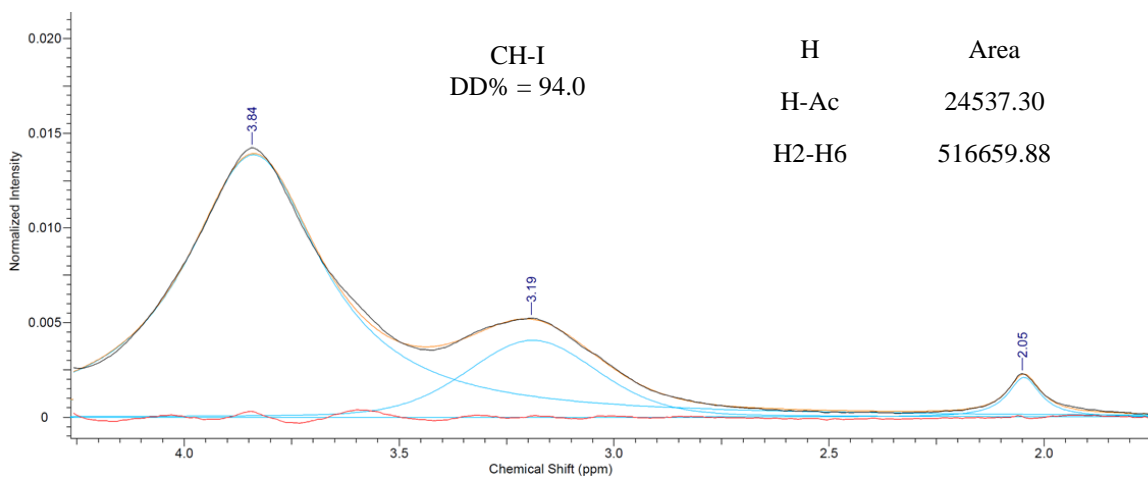


Figure 14: Deconvolution LF ^1H NMR chitosan CH-A and CH-I

6.2 Characterization of Composite Hydrogels

6.2.1 Synthesis process and Physical characteristics

During the synthesis of hydrogels, it is possible to observe the late formation of a thick uniform white solution and even the formation of a dense aggregate. This behavior is affected by the concentration of citric acid used, accelerating with increasing concentration. After the addition of CA, the material presents opposition to the agitation and cutting force.

The final shape of the hydrogel composite is reached after the ultrasound treatment. A white mass is formed whose thickness increases with the concentration of citric acid, obeying the increase in crosslinking facilitated by temperature and homogenization.

Error! Reference source not found. shown pictures of samples CMC/CH-A-CA24-G18, CMC/CH-A-CA36-G18, CMC/CH-A-CA48-G18, and CMC/CH-A-CA96-G18, a) previous and b) after ultrasound treatment. A double arrow indicates the thickness of the aggregate or lump.

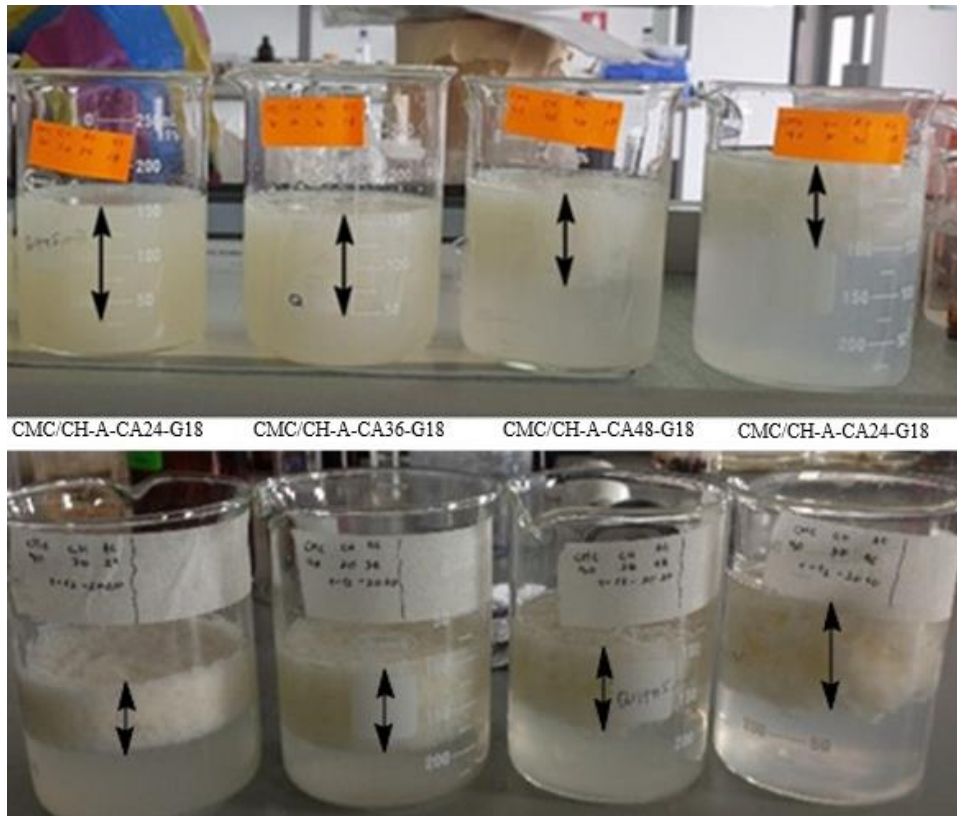


Figure 15: Behavior of AC in hydrogel composites causing a more compact matrix

Pictures of CMC/CH-A-CA24-G18, CMC/CH-A-CA36-G18, CMC/CH-A-CA48-G18, and CMC/CH-A-CA96-G18 hydrogels, before and after letting them dry at room temperature for 1 week, are shown in Figure 16.

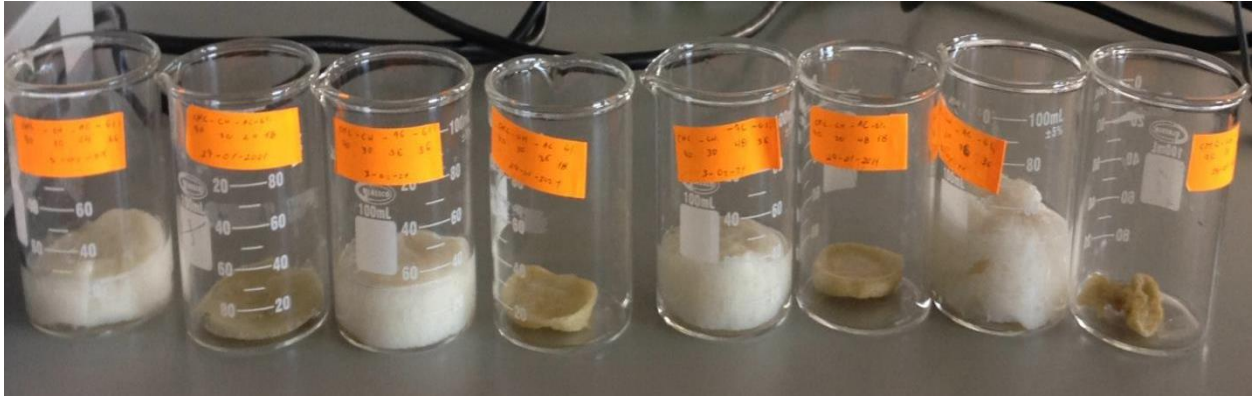


Figure 16: Composites hydrogels without drying and samples air-dried at room temperature

Figure 17 shown pictures of the composite hydrogel CMC/CH-A-CA24-G18. Its appearance is smooth and homogeneous. It presents elasticity, inherited from the biopolymer's chains. Pictures show how under pressure it can be deformed and how it returns quickly to its original shape and size after the load is removed. All the hydrogels prepared showed similar behavior.

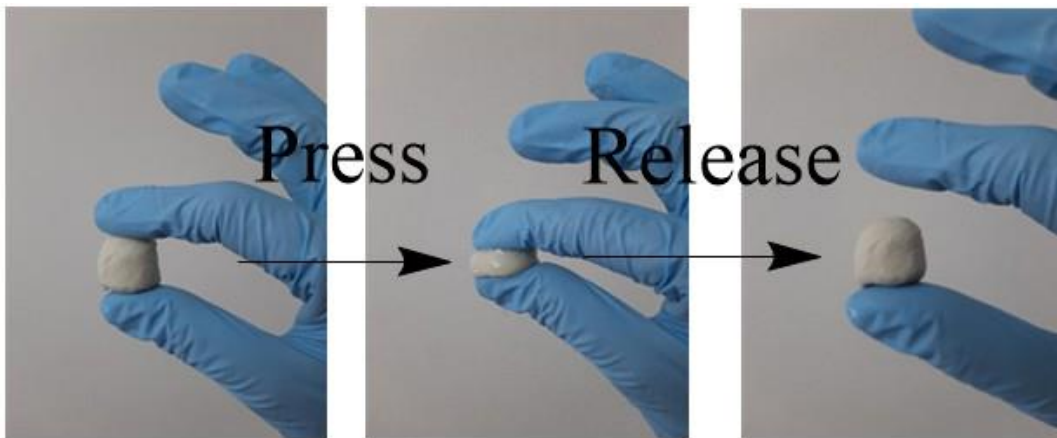


Figure 17: Behavior of AC in hydrogel composites causing a more compact matrix

The dry material suffers a significant decrease in volume and elasticity and acquire a brown tone
Figure 18.



Figure 18: CMC/CH-A-CA24-G18 without drying and samples air-dried at room temperature

6.2.2 Swelling Study

Once dried, the hydrogels were subjected to swelling tests. Swelled composites present flexibility, softness and even some of them recover the initial coloration, as shown in Figure 18 for composite CMC/CH-A-CA24-G18. In Figure 19 graphs of swelling ratio vs time are shown for CH-A and CH-I composite hydrogels, varying concentrations of glycerol and citric acid. The swelling ratios of all samples were greater than 30% after the first 5 hours. In alpha chitosan, CH-A, the equilibrium swell ratios are reached before 24 hours, and their values decrease with the citric acid concentration, showing that the increase in crosslinking decreases the swelling capacity¹⁰⁹. On the other hand, in the CH-I set, the values of swelling ratios kept changing after 24 h, thus the equilibrium swell ratio is not reached. This difference in behavior is ascribable mainly to the presence of intermolecular hydrogen bonds in alpha chitosan. Additionally, the effect of citric acid is not evident.

The higher swelling ratios were measured for CMC/CH-A-CA24-G18 and CMC/CH-I-CA24-G18, both having 18 mL of glycerol and 24 mL of CA.

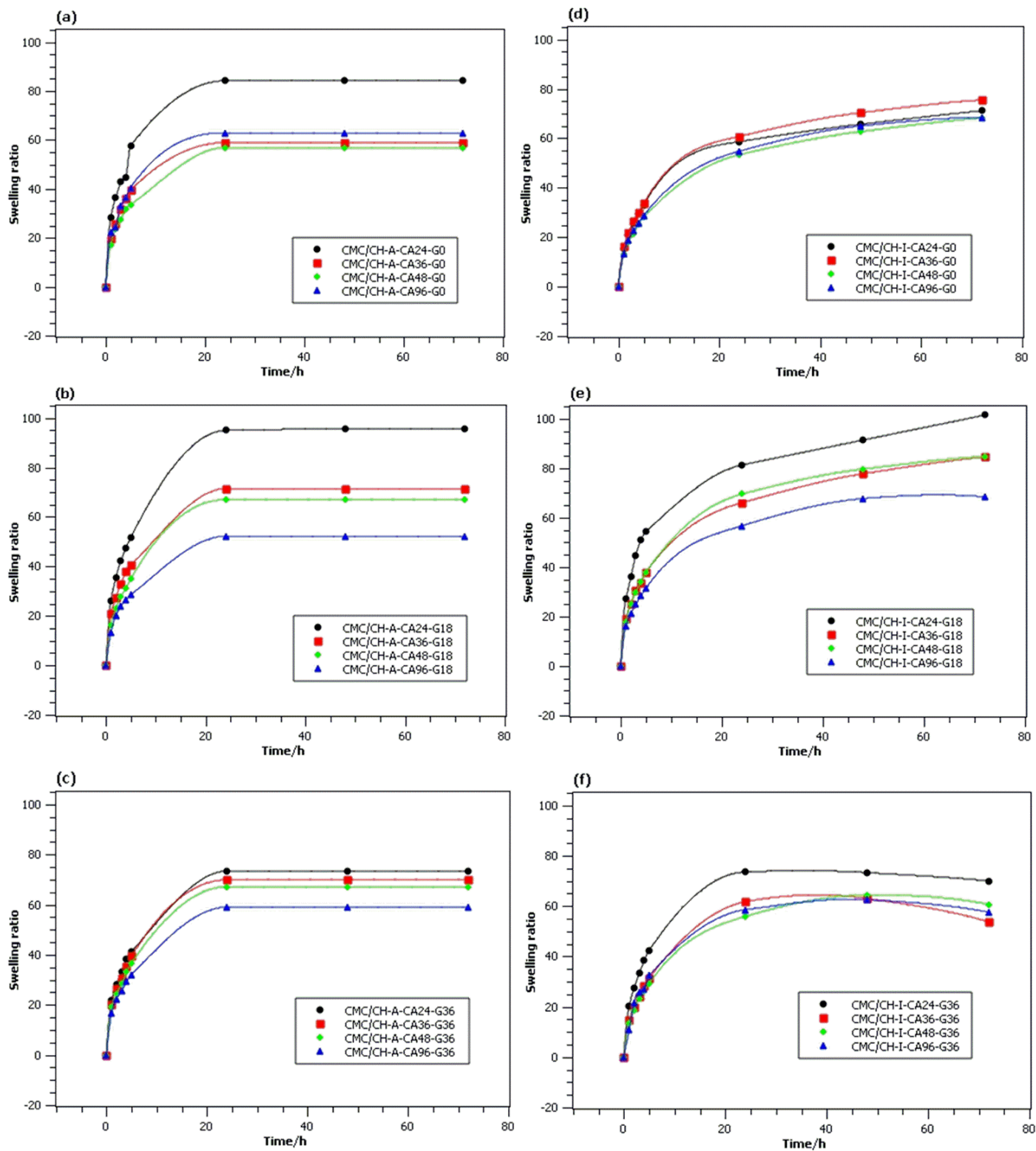


Figure 19: Swelling ratio of sponge hydrogels prepared with CH A and CH I at different ratio of glycerol and citric acid : (a)CH A-0 Glycerol,(b)CH A-18 Glycerol,(c) CH A-36 Glycerol, (d) CH I-0 Glycerol,(e)CH I-18 Glycerol and (f)CH I-36 Glycerol.

6.2.3 X-ray Diffraction

Figure 20 shows X-ray diffraction patterns of (a) CMC, (b) CH-A, and (c) CH-A composites hydrogels with different CA concentrations. A strong peak at $2\theta \approx 21^\circ$ characteristic of the polysaccharide is observed for all the samples¹¹⁰. CH-A exhibits two crystalline peaks at $2\theta \approx 10.8^\circ$ and $2\theta \approx 20.0^\circ$ due to X-ray diffraction of the (020) and (110) planes of the semi-crystalline α -chitosan powder. XRD patterns in Figure 20 (c) show the gradual disappearance of the signal around $2\theta \approx 10.0$, and a broadening in general of the peaks, with CA concentration. These results indicate a loss of crystallinity due to crosslinking caused by CA because it restricts the movement in the polysaccharide chains¹⁰⁹.

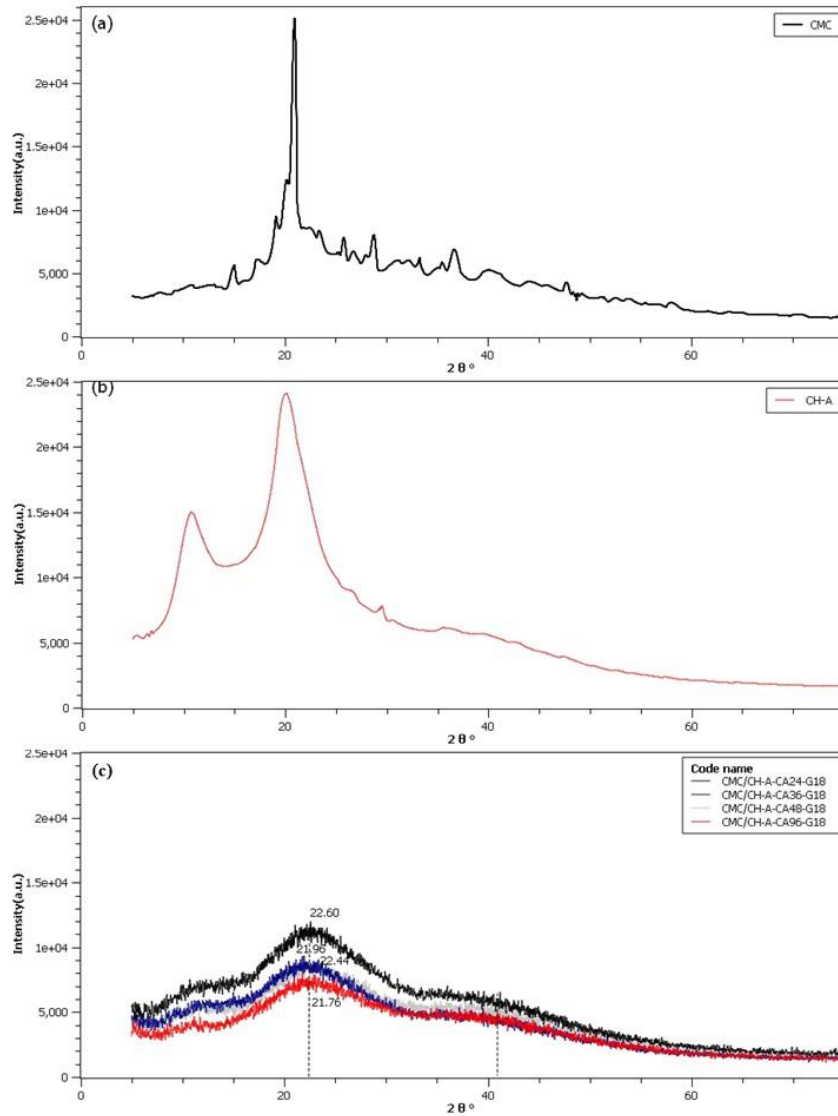


Figure 20: XRD(a)CMC,(b)CH-A and (c) CH A-18 Glycerol.

6.2.4 Fourier Transform Infrared Spectroscopy - Attenuated Total Reflectance

Figure 21 shows FT-IR spectra of composites hydrogels prepared with CH-A and CH-I at different ratios of glycerol and citric acid. All the spectra were similar to each other, showing the characteristic bands of the chitosan and CMC, with an additional signal at 1725 cm^{-1} . The intensity of this additional signal shows a correlation with the concentration of citric acid; as the CA concentration increases so does the intensity of the signal. According to the literature, this signal is related to the formation of ester bonds caused by the esterification reaction between CMC and CA^{109,111,112} and the increase in intensity corresponds to an increase in the degree of chemical crosslinking.

Figure 22 offers an enlargement of the region corresponding from 1400 to 1800 cm^{-1} range for the samples: CMC/CH-A-CA24-G18, CMC/CH-A-CA36-G18, CMC/CH-A-CA48-G18, CMC/CH-A-CA96-G18, and the reagents chitosan & CMC. In both the CMC and chitosan, a band is present at 1585 cm^{-1} . This band is associated with the symmetric stretching vibrations of the COO- groups in the case of CMC and corresponds to N-H bending vibration of -NH₂ groups in chitosan. In the composites hydrogels spectra, this band has shifted to 1576 cm^{-1} , suggesting an ionic interactions and/or hydrogen bonds between the chitosan and the CMC. It is possible that hydrogen bridge interaction between the chitosan and CA are also a factor in this shift.

The FT-IR results discussed in this section seem to indicate that the composites hydrogels have successfully undergone chemical and physical crosslinking¹¹³.

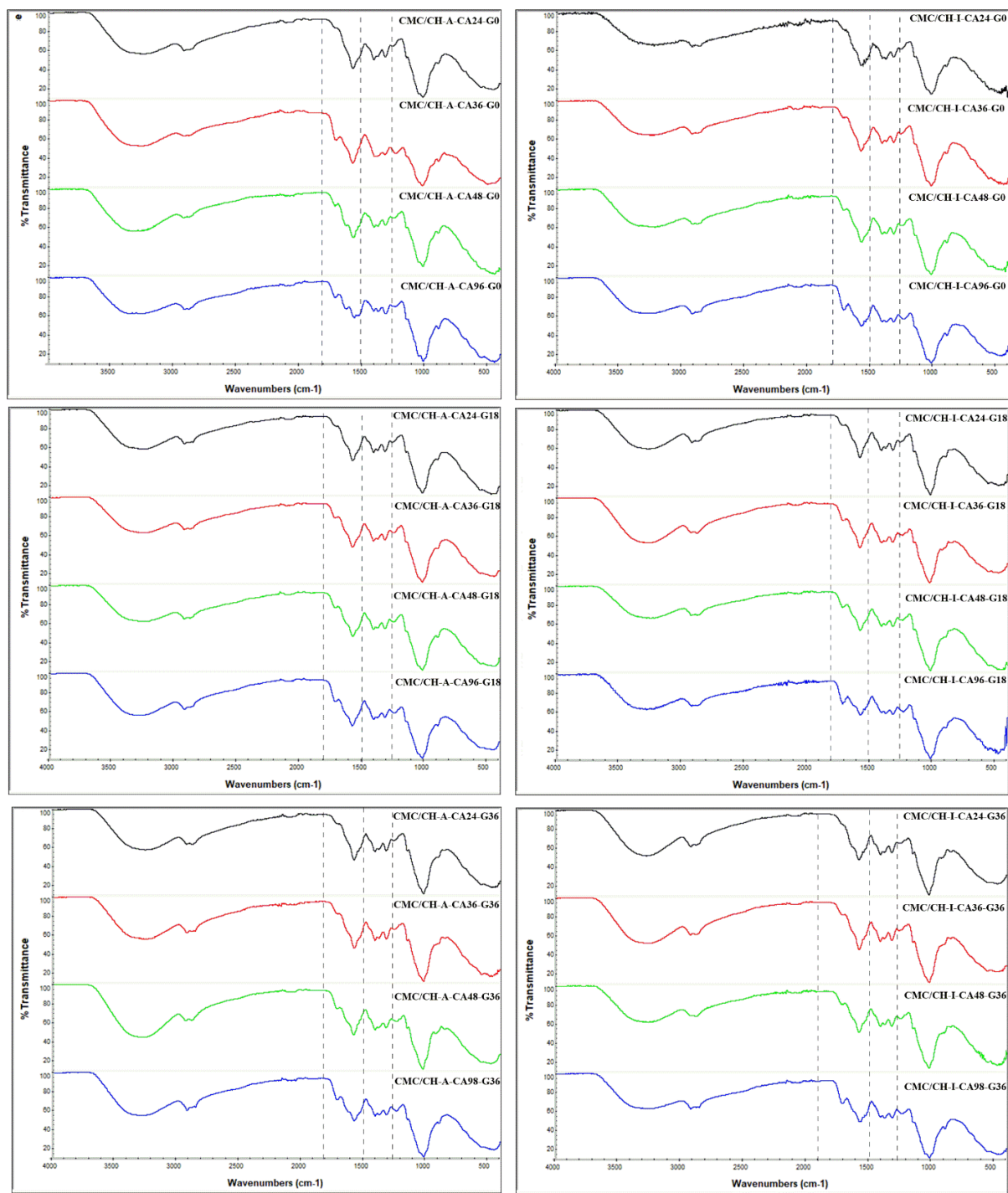


Figure 21: FT-IR of composites hydrogels prepared with CH A and CH I at different ratio of glycerol and citric acid : (a)CH A-0 Glycerol,(b)CH A-18 Glycerol,(c) CH A-36 Glycerol, (d) CH I-0 Glycerol,(e)CH I-18 and (f)CH I-18.

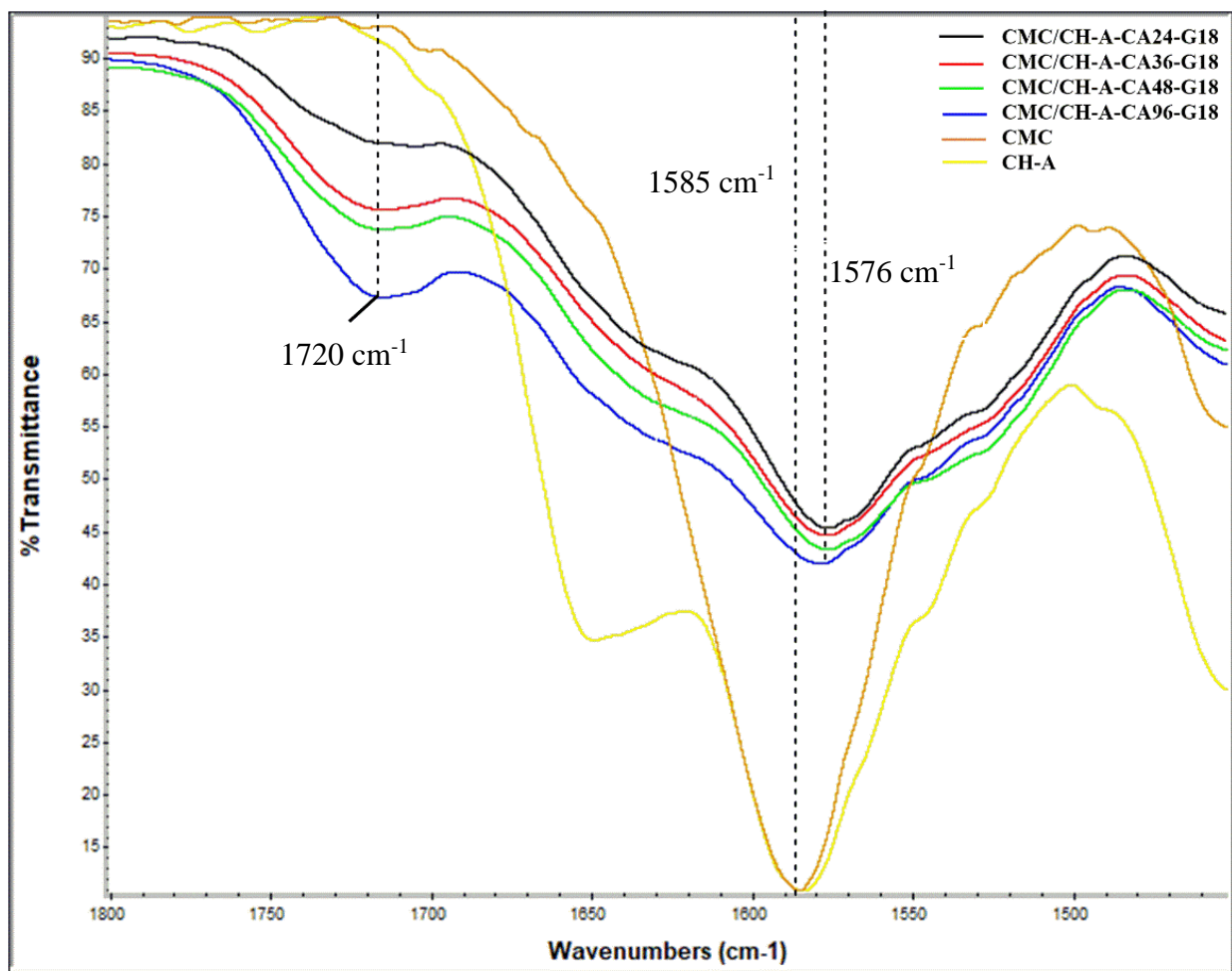


Figure 22: FTIR composites hydrogels matrices at different ratios of CA, CMC, and CH A-18 Glycerol.

6.2.5 Differential Scanning Calorimetry

Figure 23 presents the results of DSC heating analysis belonging to the sample CMC / CH-CA48-GL18. In the first heating from 20 C° to 120 C° shown in Figure 23.a, a loss of water can be observed at 60 C°, this loss is caused by the dehydration of citric acid that produces the formation of anhydride³⁶. A second heating from 20 C° to 200 C° (see Figure 23.b) showed no glass transition temperature (T_g) which suggests that the composites hydrogel has a glass transition over 200 C°¹⁰⁹. Previous DSC studies have reported T_g values in the range 200 to 203 C° for CH^{114,115}, while for CMC T_g values from 79 to 80C°¹⁶. The sample studied has chemical crosslinking which increase the T_g¹⁰⁹, due to the van der Waals interactions are replaced by covalent bonds in this specific case ester and amide bonds. The hydrogel composition has a composition of 3: 1

respectively for CMC / CH and a concentrated amount of CA, therefore the material must present a unified behavior.

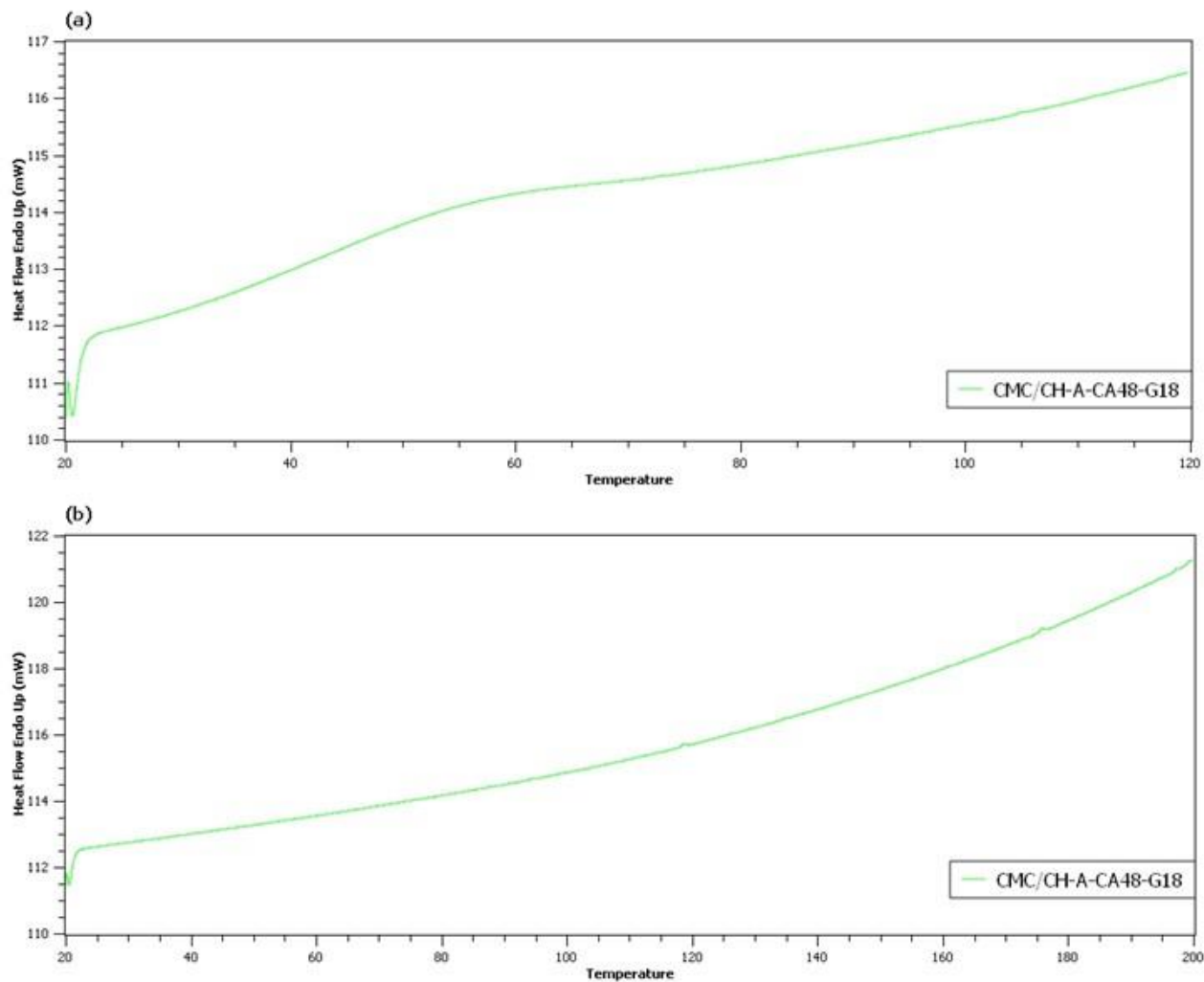


Figure 23: DSC analysis of CMC/CH-CA48-GL18 : (a)first heating from 20 C° to 120 C°, (b)second heating of 20 C° to 200C°

6.2.6 X-ray Photoelectron Spectroscopy

The survey spectra of both chitosan -A, -I, and CH-A -18 composites, shown in Figure 24, exhibit the characteristic peaks at 285 eV (C1s) and 400 eV (N1s). The values from the analysis of the spectra are tabulated in Table 5.

The high-resolution spectra recordings of C1s were obtained and peak fitting using Gaussian-Lorentzian functions were performed to obtain a piece of more detailed information. Figure 25,

shows 3 peaks for CH-A associated with the following values: 284.3, 286.2, 287.4 eV, corresponding to the following bonds: -C-C-/C-H-, -C-N-/C-O-/C-O-H and -C=O-/O-C-O-/N-C=O^{68,116}. On the other hand, composite hydrogels present signals to: 285.0, 286.7, 288.3, and 289 eV, corresponding to the following bonds: C-C / C-H, -C-N, -COO⁻, -COOH^{116,117,118}. Table 6 shows more individual details of C1s belonging to CH-A and composites. The complexity of these samples and the resulting overlapping of signals makes difficult any conclusion from C1s spectra.

N1s high resolution spectrum of CH-A shown in Figure 26 exhibit one peak at 400.0 eV associated with the following bonds: -NH₂ and -O-C-N^{119,120}. Table 7 shows more individual details of N1s belonging to CH-A. The fitting of N1s spectra of all the hydrogel composites was resolved with two peaks, shown in Figure 25, centered about: 400 and 402 eV, corresponding to the following bonds: O-C-N and NH₃⁺^{7,120,121}. The N1s spectra show the disappearance of the -N-H groups and the increase of O-C-N and NH₃⁺ groups with CA concentration, due to the formation of covalent crosslinks (amides), ionic interactions and/or hydrogen bonds⁷. Table 7: shows more individual details of N1s belonging to CH-A-18 Glycerol.

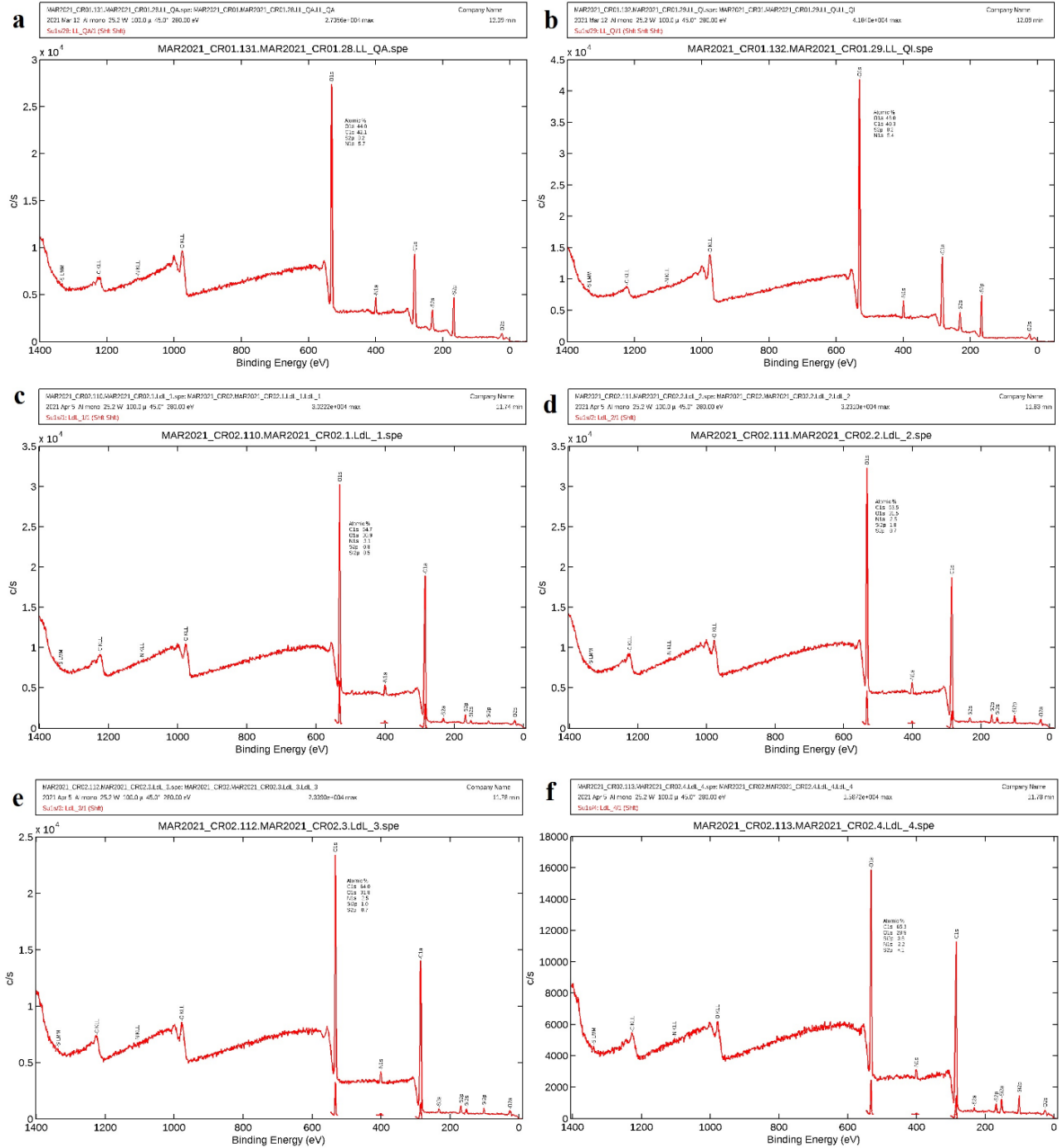


Figure 24: Survey XPS of (a)CH-A, (b)CH-I,(c) CMC/CH-A-CA24-G18,(d) CMC/CH-A-CA36-G18,(e) CMC/CH-A-CA48-G18 and,(e) CMC/CH-A-CA96-G18.

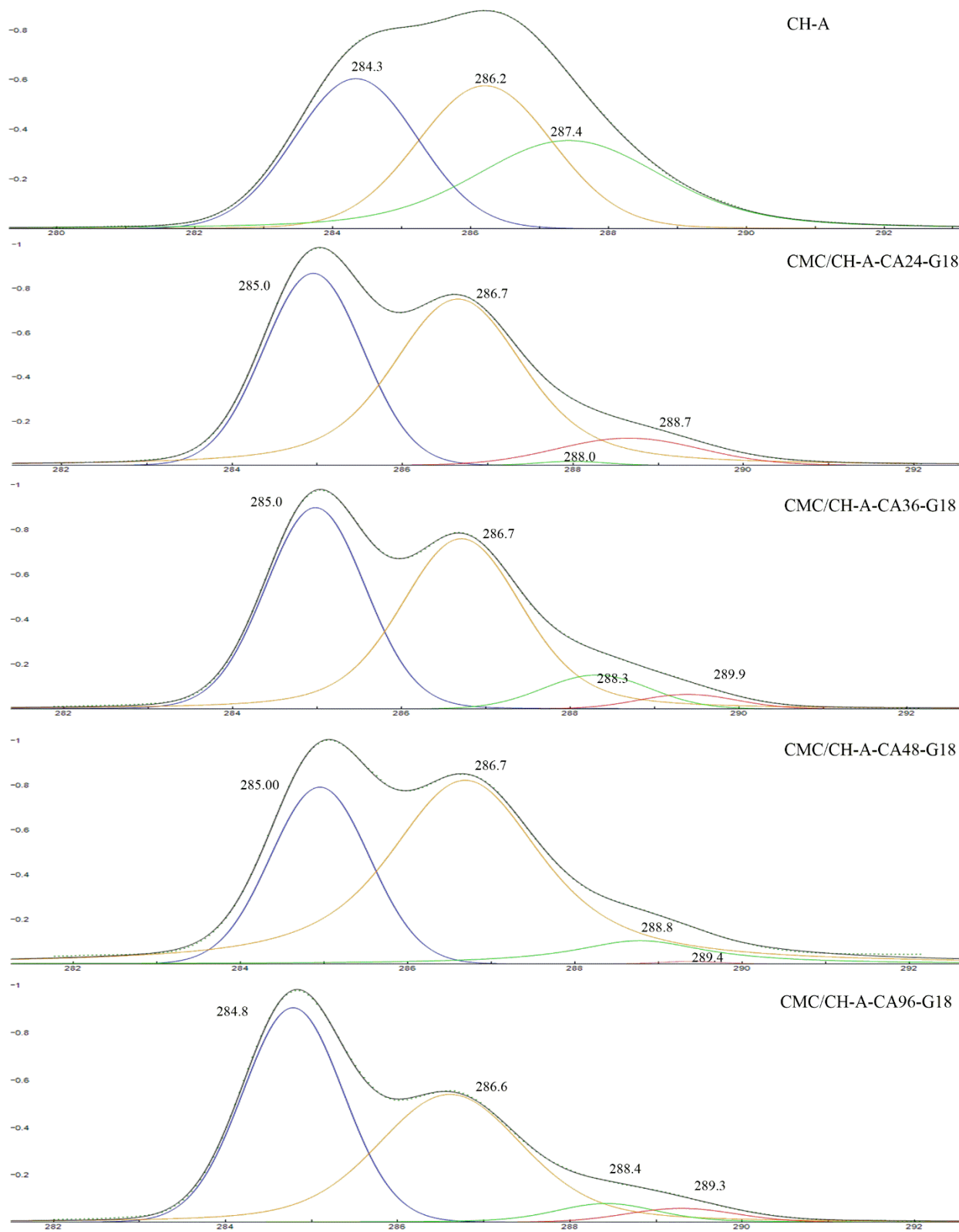


Figure 25: Survey XPS of C1s spectrum CH-A and CH A-18 Glycerol composites hydrogels

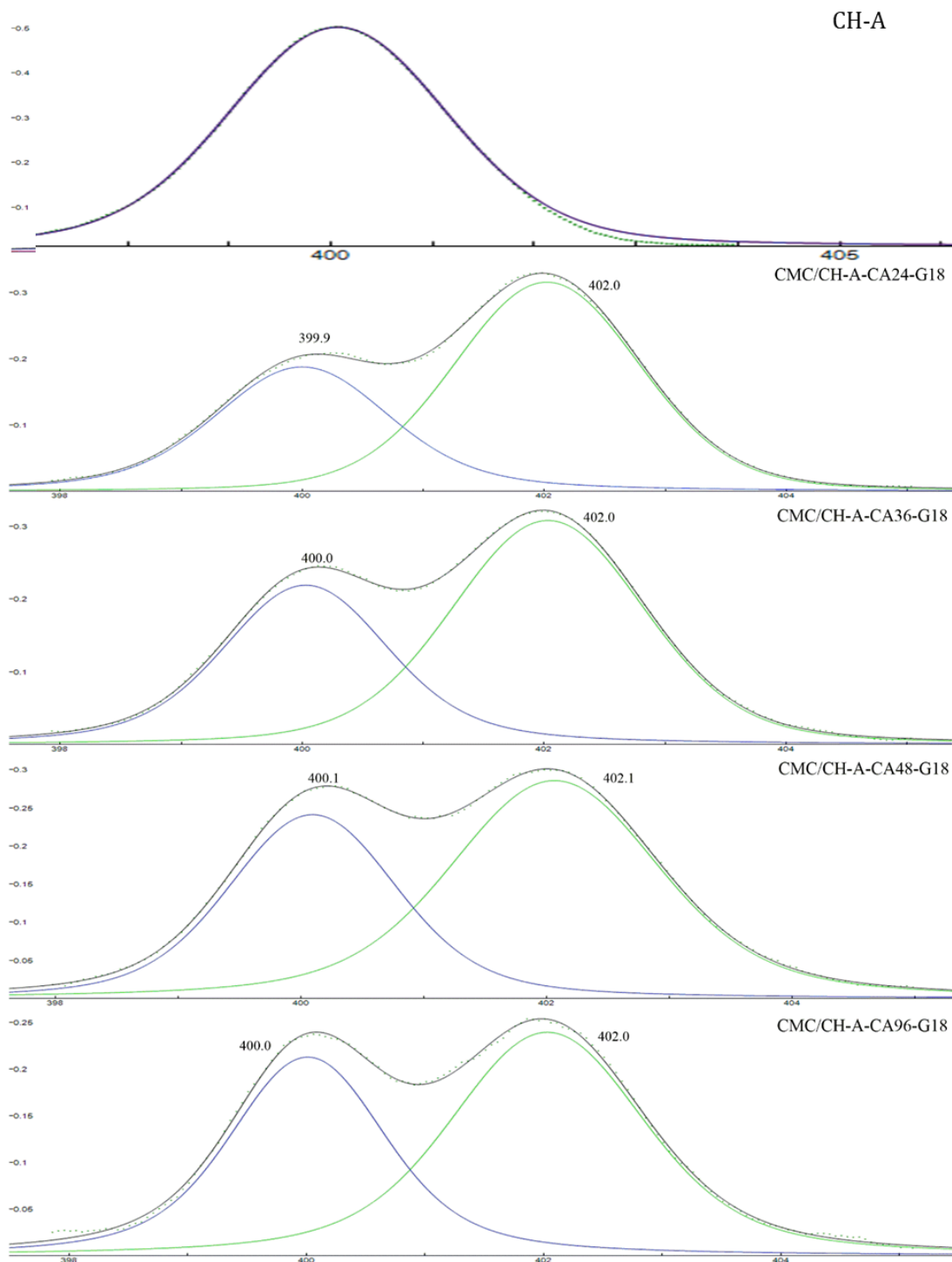


Figure 26: Survey XPS of Ni spectrum CH-A and CH-A-18 Glycerol composites hydrogels

<u>Sample</u>	<u>C(%)</u>	<u>O(%)</u>	<u>N(%)</u>
CH-A	42	44	5.7
CH-I	40.3	46	5.4
CMC/CH-A-CA24-G18	64.7	30.9	3.1
CMC/CH-A-CA36-G18	63.5	31.5	2.5
CMC/CH-A-CA48-G18	64.0	31.8	2.5
CMC/CH-A-CA96-G18	65.3	28.9	3.6

Table 5: Surface elemental compositions of CH-A, CH-I, and CH A-18 Glycerol composites hydrogels

<u>XPS</u>	<u>Sample</u>	<u>Possible element state</u>	<u>Position(eV)</u>	<u>Area</u>	<u>Area %</u>	<u>Height</u>
C1s	CH-A	CC / HH	284.339	1.346	32.098	0.603
		C-NH	286.211	1.452	34.615	0.575
		COC = O / C-OH	287.425	1.396	33.287	1.396
C1s	CMC/CH-A-CA24-G18	C-C / C-H	284.954	1.267	38.475	0.868
		-C-N	286.652	1.749	53.114	0.751
		-COO ⁻	287.992	0.017	0.529	0.018
		-COOH	288.653	0.260	7.881	0.123
C1s	CMC/CH-A-CA36-G18	C-C / C-H	284.980	1.362	41.613	0.898
		-C-N	286.712	1.577	48.163	0.760
		-COO ⁻	288.313	0.240	7.329	0.151
		-COOH	289.393	0.095	2.896	0.065
C1s	CMC/CH-A-CA48-G18	C-C / C-H	284.952	1.177	29.586	0.789

		-C-N	286.690	2.479	62.315	0.820
		-COO ⁻	288.778	0.311	7.829	0.104
		-COOH	289.381	0.011	0.270	0.011
	CMC/CH-A-CA96-					
C1s	G18	C-C / C-H	284.785	1.329	46.605	0.905
		-C-N	286.607	1.297	45.487	0.539
		-COO ⁻	288.422	0.133	4.664	0.079
		-COOH	289.293	0.093	3.244	0.058

Table 6: Relative intensities of the fitted C1s peak of CH-A and CH A-18 Glycerol composites hydrogels

<u>XPS</u>	<u>Sample</u>	<u>Possible element state</u>	<u>Position(eV)</u>	<u>Area</u>	<u>Area %</u>	<u>Height</u>
N1s	CH-A	-NH ₂ /O-C-N	400.030	1.000	100	1.000
	CMC/CH-A-CA24-					
N1s	G18	O-C-N	399.999	0.396	37.863	0.187
		NH ₃ ⁺	402.021	0.651	62.137	0.315
	CMC/CH-A-CA36-					
N1s	G18	O-C-N	400.030	0.439	39.374	0.219
		NH ₃ ⁺	402.033	0.676	60.626	0.308
	CMC/CH-A-CA48-					
N1s	G18	O-C-N	400.096	0.478	40.044	0.241
		NH ₃ ⁺	402.064	0.715	59.956	0.286
	CMC/CH-A-CA96-					
N1s	G18	O-C-N	400.013	0.424	42.065	0.213
		NH ₃ ⁺	402.032	0.584	57.935	0.239

Table 7: Relative intensities of the fitted N 1s peak of CH-A and CH A-18 Glycerol composites hydrogels

6.2.7 Morphology Study

Figure 27 and Figure 28 show stereomicrographs and SEM micrographs of the CH A-18 Glycerol composite hydrogels, respectively. A heterogenous porous distribution, with only the presence of macropores and no visible porous interconnectivity can be observed. In both stereomicrographs, spherical cavities can be observed, their presence can be explained by: firstly, the electrostatic interactions between polymer molecules; secondly, formation of large aggregates; and finally, the action of surface and stirring force¹²². These cavities are filled with free water and become empty after evaporation during the drying process. In stereomicrograph (b), corresponding to a hydrogel with a higher citric acid concentration, shows replacement of spherical cavities for region of laminar surfaces. This is due to the increase in chemical crosslinking caused by the higher concentration of citric acid. In the other hand, the roughness observed in SEM micrographs is probably related to the strong intermolecular hydrogen bonds between CMC and chitosan which might give rise to a chaotic gel state in the solution that leads to a rough surface⁴⁷.

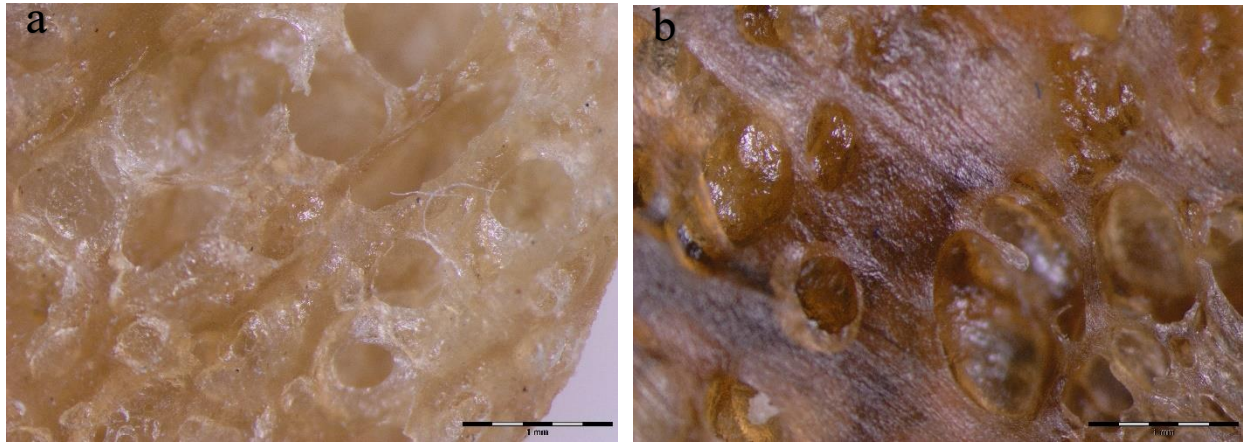


Figure 27. Stereomicrographs at x2.5 magnification of (a) CH/CMC-CA36-G18 (b) CH/CMC-CA96-G18

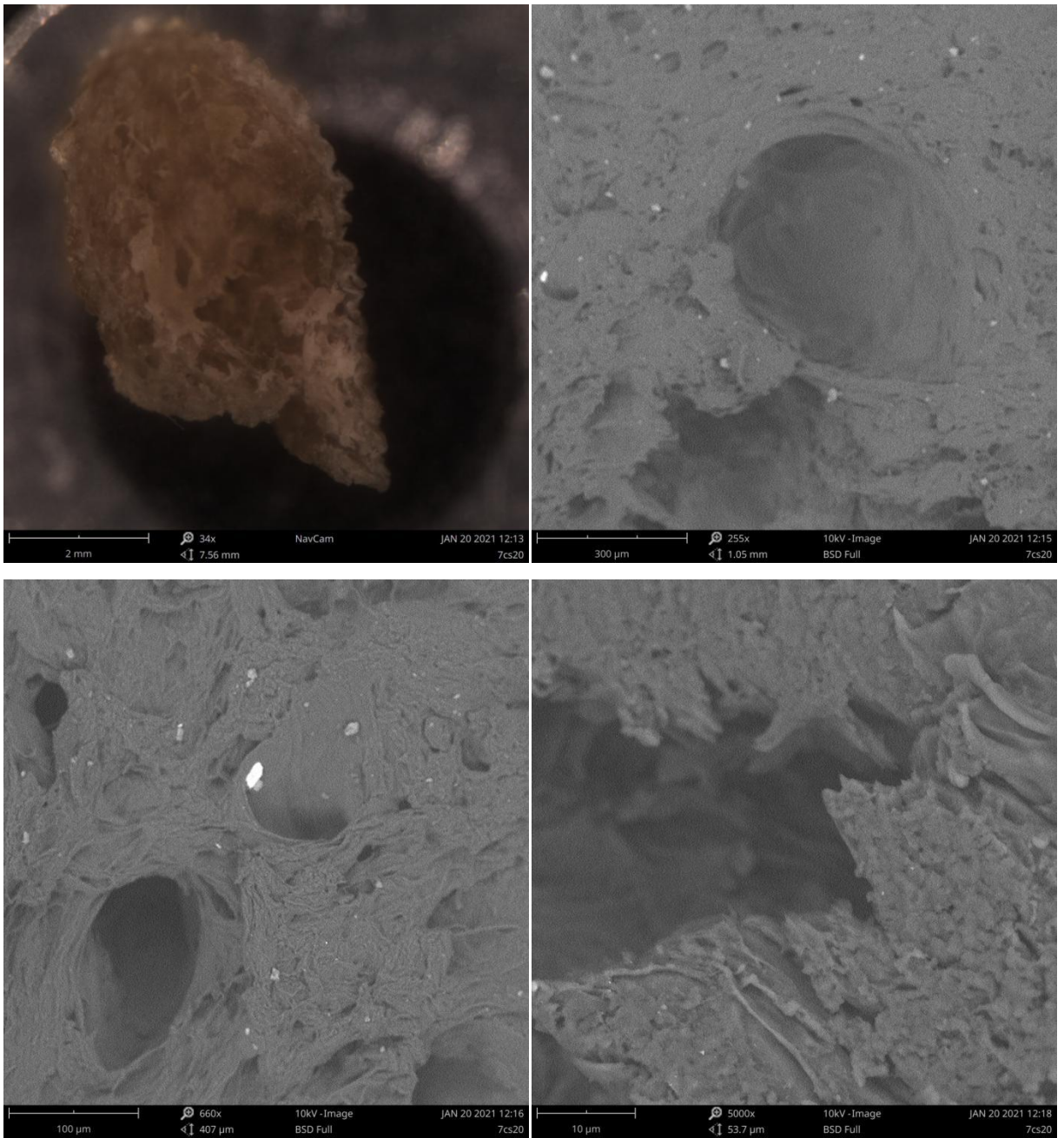


Figure 28: SEM micrographs of the transversal surfaces of CH A-18 Glycerol with the following magnifications (a) 2mm, (b) 100μm, (c) 100μm, and (d) 10μm

6.2.8 A Suggested Chemical Structure of the composite Hydrogels

Based on the different chemical characterizations carried out, where chemical and physical crosslinking was confirmed. We are proposing an average chemical structure of the composite hydrogel. Figure 29 illustrates a proposed reaction equation of the composite hydrogel's formation.

The following spectroscopic observations supported the proposed average structure for the hydrogels:

- The presence of a signal at 1725 cm^{-1} in the composites FT-IR spectra confirms ester bonds formation. A positive correlation of the intensity of this signal with the CA concentration suggest that the ester bonds are forming between CMC and CA ^{109,111,112,123}.
- A red shift of the signal at 1585 cm^{-1} (N-H bending vibration of $-\text{NH}_2$ groups in chitosan and symmetric stretching vibrations of the COO^- groups in the case of CMC) to 1576 cm^{-1} can be attribute to the physical interaction between COO^- groups of CMC and NH_3^+ groups of chitosan^{113,117}, suggesting an ionic interaction and/or hydrogen bridge between the chitosan and the CMC.
- N1s high resolution spectra of composites indicate that the amine groups of chitosan are protonated (NH_3^+) ^{7,120,121}.
- The increase of the number of O-C-N bond groups with CA concentration in the XPS spectra of composites could be ascribed to the formation of covalent crosslinks between the amine group of chitosan and CA ^{7,117}. However, we can not reject the possibility of ester bonds between CMC and chitosan.
- There is no evidence of esterification between C-6 carbon of chitosan and CA.

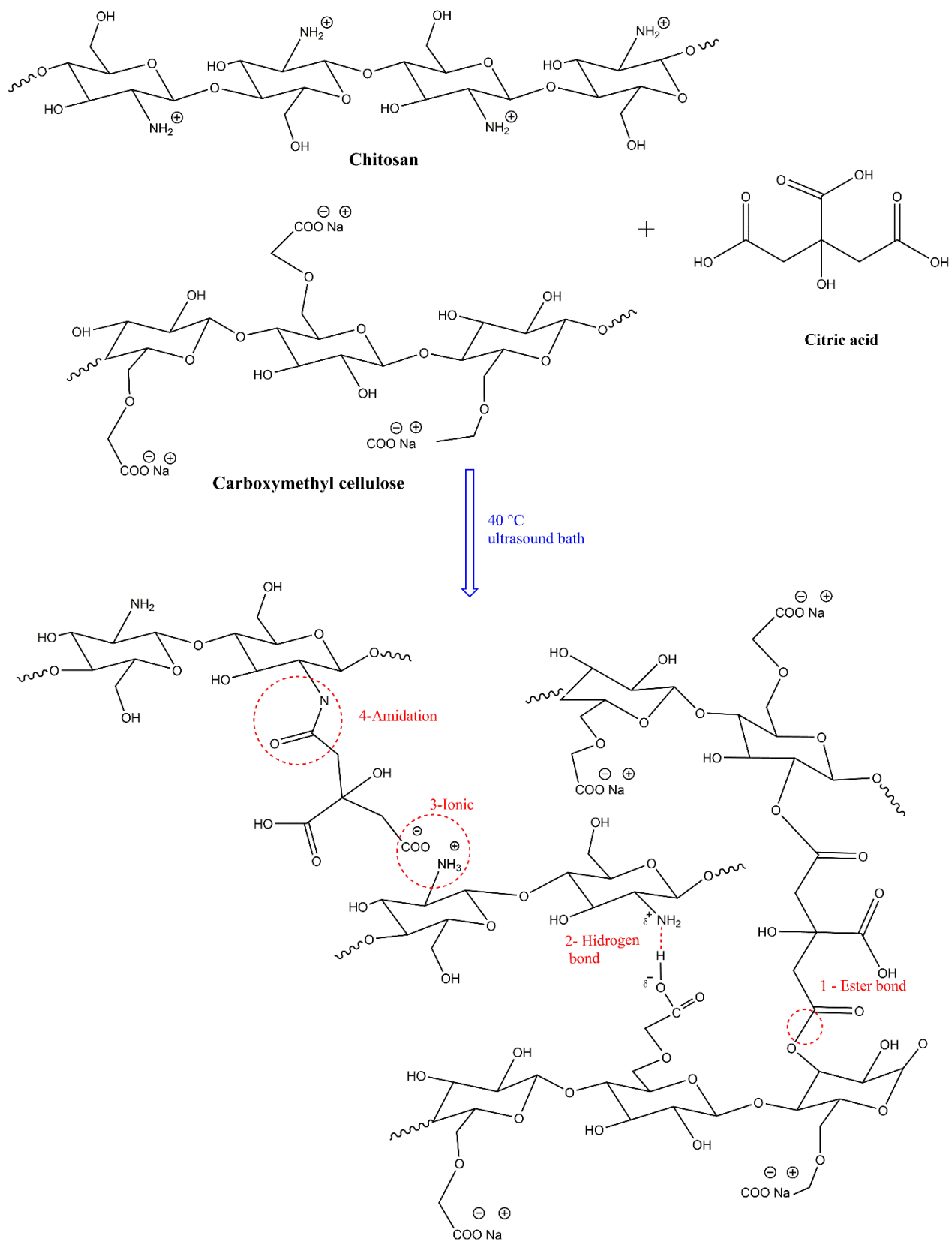


Figure 29: Reaction equation of the composites hydrogels formation..

7 CONCLUSIONS AND RECOMMENDATIONS

A green methodology was successfully developed to produce composite hydrogels using only environmentally friendly materials. Citric acid turned out to be an effective chemical crosslinker promoting formations of amide and ester bonds between chitosan and carboxymethyl cellulose. A synergetic effect between glycerol and citric acid was evident in the swelling study, the highest equilibrium swelling ratio percentage was obtained at a specific combination of the two. Chitosan alpha was able to swell when combined with glycerol indicating a disruption in the intermolecular hydrogen bonding. The swelled hydrogels presented a smooth and homogeneous appearance, with the presence of macropores and elastic behavior. However, once they were dried, the material lost its elasticity, became rigid and difficult to shear. The dried hydrogels showed no glass transition under 200 C° and a loss of crystallinity due to crosslinking caused by citric acid.

Current hydrogel research reports the use of materials with similar properties to the ones obtained in this study for applications such as: adsorption of heavy metals, hemostasis in animals, regeneration of bone tissue, and wound healing. Therefore, it is recommended to carry out further studies into the properties of our hydrogel to be able to propose specific applications. Incorporate freeze-dried methodology to improve pore distribution, increase interconnectivity, and reach mesoporosity and microporosity.

BIBLIOGRAPHY

1. *Cellulose-Based Superabsorbent Hydrogels*. (Springer International Publishing, 2019). doi:10.1007/978-3-319-77830-3.
2. Caló, E. & Khutoryanskiy, V. V. Biomedical applications of hydrogels: A review of patents and commercial products. *European Polymer Journal* vol. 65 252–267 (2015).
3. Wang, H., Li, D., Yano, H. & Abe, K. Preparation of tough cellulose II nanofibers with high thermal stability from wood. *Cellulose* **21**, 1505–1515 (2014).
4. Ergun, R., Guo, J. & Huebner-Keese, B. Cellulose. in (eds. Caballero, B., Finglas, P. M. & Toldrá, F. B. T.-E. of F. and H.) 694–702 (Academic Press, 2016). doi:<https://doi.org/10.1016/B978-0-12-384947-2.00127-6>.
5. Ergun, R., Guo, J. & Huebner-Keese, B. Cellulose. in *Encyclopedia of Food and Health* 694–702 (Elsevier Inc., 2015). doi:10.1016/B978-0-12-384947-2.00127-6.
6. Narang, A. S. & Badawy, S. I. F. *Handbook of pharmaceutical wet granulation: Theory and practice in a quality by design paradigm. Handbook of Pharmaceutical Wet Granulation: Theory and Practice in a Quality by Design Paradigm* (Elsevier, 2018). doi:10.1016/C2016-0-00287-5.
7. Zhi, X., Du, B. & Yuan, S. Preparation of Elastic and Antibacterial Chitosan–Citric Membranes with High Oxygen Barrier Ability by in Situ Cross-Linking. *ACS Omega* **XXXX**, (2020).
8. CNA/EL COMERCIO. El camarón alcanzó cifra récord en el 2019 | El Comercio. *El camarón alcanzó cifra récord en el 2019 en el Ecuador* <https://www.elcomercio.com/actualidad/camaron-record-ecuador-exportacion-economia.html> (2020).
9. Varun, T. K. *et al.* Extraction of chitosan and its oligomers from shrimp shell waste, their characterization and antimicrobial effect. *Vet. world* **10**, 170–175 (2017).
10. Iqbal, A. Production and characterization of Chitosan from shrimp waste. *J. Bangladesh Agric. Univ.* **12**, (2015).

11. Cheng, K.-C., Huang, C.-F., Wei, Y. & Hsu, S. Novel chitosan–cellulose nanofiber self-healing hydrogels to correlate self-healing properties of hydrogels with neural regeneration effects. *NPG Asia Mater.* **11**, 25 (2019).
12. Huang, W. *et al.* Stretchable, tough, self-recoverable, and cytocompatible chitosan/cellulose nanocrystals/polyacrylamide hybrid hydrogels. *Carbohydr. Polym.* **222**, 114977 (2019).
13. George, D., Maheswari, P. & Begum, M. Synergic formulation of onion peel quercetin loaded chitosan-cellulose hydrogel with green zinc oxide nanoparticles towards controlled release, biocompatibility, antimicrobial and anticancer activity. *Int. J. Biol. Macromol.* **132**, (2019).
14. Uyanga, K. A., Okpozo, O. P., Onyekwere, O. S. & Daoud, W. A. Citric acid crosslinked natural bi-polymer-based composite hydrogels: Effect of polymer ratio and beta-cyclodextrin on hydrogel microstructure. *React. Funct. Polym.* **154**, 104682 (2020).
15. Alavi, M. & Nokhodchi, A. An overview on antimicrobial and wound healing properties of ZnO nanobiofilms, hydrogels, and bionanocomposites based on cellulose, chitosan, and alginate polymers. *Carbohydr. Polym.* **227**, 115349 (2019).
16. Basu, P., Narendrakumar, U., Arunachalam, R., Devi, S. & Manjubala, I. Characterization and Evaluation of Carboxymethyl Cellulose-Based Films for Healing of Full-Thickness Wounds in Normal and Diabetic Rats. *ACS Omega* **3**, 12622–12632 (2018).
17. Carvalho, S. M. *et al.* Synthesis and in vitro assessment of anticancer hydrogels composed by carboxymethylcellulose-doxorubicin as potential transdermal delivery systems for treatment of skin cancer. *J. Mol. Liq.* **266**, 425–440 (2018).
18. Shariatnia, Z. Carboxymethyl chitosan: Properties and biomedical applications. *Int. J. Biol. Macromol.* **120**, 1406–1419 (2018).
19. Zhang, L. *et al.* A composite hydrogel of chitosan/heparin/poly (γ -glutamic acid) loaded with superoxide dismutase for wound healing. *Carbohydr. Polym.* **180**, 168–174 (2018).
20. Wang, L. *et al.* A natural polymer-based porous sponge with capillary-mimicking microchannels for rapid hemostasis. *Acta Biomater.* **114**, 193–205 (2020).

21. Tu, C., Zhang, R., Yan, C., Guo, Y. & Cui, L. A pH indicating carboxymethyl cellulose/chitosan sponge for visual monitoring of wound healing. *Cellulose* **26**, 4541–4552 (2019).
22. Nguyen, M. A. & Camci-Unal, G. Unconventional Tissue Engineering Materials in Disguise. *Trends in Biotechnology* vol. 38 178–190 (2020).
23. Kaufman, M. Otto Wichterle, 84, químico que hizo los primeros contactos blandos - The New York Times. a-29 <https://www.nytimes.com/1998/08/19/business/otto-wichterle-84-chemist-who-made-first-soft-contacts.html> (1998).
24. Wang, H. *et al.* Effect of Ethylenediamine Treatment on Cellulose Nanofibers and the Formation of High-strength Hydrogels. (2019) doi:10.15376/biores.14.1.1141-1156.
25. Araki, J. & Miyayama, M. Wet spinning of cellulose nanowhiskers; fiber yarns obtained only from colloidal cellulose crystals. *Polymer (Guildf)*. **188**, 122116 (2020).
26. Wang, H. *et al.* A Comparative Study on the Characterization of Nanofibers with Cellulose I, I/II, and II Polymorphs from Wood. *Polymers (Basel)*. **11**, 153 (2019).
27. Oliveira, J. P. de *et al.* Cellulose fibers extracted from rice and oat husks and their application in hydrogel. *Food Chem.* **221**, 153–160 (2017).
28. Loix, C. *et al.* Reciprocal interactions between cadmium-induced cell wall responses and oxidative stress in plants. *Frontiers in Plant Science* vol. 8 (2017).
29. Holtzapple, M. T. CELLULOSE. in *Encyclopedia of Food Sciences and Nutrition* 998–1007 (Elsevier, 2003). doi:10.1016/B0-12-227055-X/00185-1.
30. Wada, M., Heux, L. & Sugiyama, J. Polymorphism of cellulose I family: Reinvestigation of cellulose IVI. *Biomacromolecules* **5**, 1385–1391 (2004).
31. Kanikireddy, V., Varaprasad, K., Jayaramudu, T., Karthikeyan, C. & Sadiku, R. Carboxymethyl cellulose-based materials for infection control and wound healing: A review. *Int. J. Biol. Macromol.* **164**, 963–975 (2020).
32. Ahmed Reem, T. E. A. Synthesis and Characterization of Carboxymethylcellulose (CMC) from Rice husk. (Sudan University of Science and Technology, 2016).

33. Stigsson, V., Kloow, G. & Germgård, U. An historic overview of carboxymethyl cellulose (CMC) production on an industrial scale. *PaperAsia* **vol 17, no**, (2001).
34. (PDF) Microwave synthesis of Carboxymethylcellulose (CMC) from Rice Husk. https://www.researchgate.net/publication/342165164_Microwave_synthesis_of_Carboxymethylcellulose_CMC_from_Rice_Husk.
35. Mali, K., Dhawale, S., Dias, R., Dhane, N. & Ghorpade, V. Citric Acid Crosslinked Carboxymethyl Cellulose-based Composite Hydrogel Films for Drug Delivery. *Indian J. Pharm. Sci.* **80**, 657–667 (2018).
36. Demitri, C. *et al.* Novel superabsorbent cellulose-based hydrogels crosslinked with citric acid. *J. Appl. Polym. Sci.* **110**, 2453–2460 (2008).
37. Barbosa, M. A., Granja, P. L., Barrias, C. C. & Amaral, I. F. Polysaccharides as scaffolds for bone regeneration. *ITBM-RBM* **26**, 212–217 (2005).
38. Abd El-Hack, M. E. *et al.* Antimicrobial and antioxidant properties of chitosan and its derivatives and their applications: A review. *Int. J. Biol. Macromol.* **164**, 2726–2744 (2020).
39. Muxika, A., Etxabide, A., Uranga, J., Guerrero, P. & de la Caba, K. Chitosan as a bioactive polymer: Processing, properties and applications. *Int. J. Biol. Macromol.* **105**, 1358–1368 (2017).
40. Van Vlierberghe, S., Dubruel, P. & Schacht, E. Biopolymer-Based Hydrogels As Scaffolds for Tissue Engineering Applications: A Review. *Biomacromolecules* **12**, 1387–1408 (2011).
41. Ribeiro, J. C. V., Vieira, R. S., Melo, I. M., Araújo, V. M. A. & Lima, V. Versatility of Chitosan-Based Biomaterials and Their Use as Scaffolds for Tissue Regeneration. *Sci. World J.* **2017**, 8639898 (2017).
42. Peniche, C., Argüelles-Monal, W. & Goycoolea, F. M. Chapter 25 - Chitin and Chitosan: Major Sources, Properties and Applications. in (eds. Belgacem, M. N. & Gandini Polymers and Composites from Renewable Resources, A. B. T.-M.) 517–542 (Elsevier, 2008). doi:<https://doi.org/10.1016/B978-0-08-045316-3.00025-9>.

43. Kou, S. (Gabriel), Peters, L. M. & Mucalo, M. R. Chitosan: A review of sources and preparation methods. *Int. J. Biol. Macromol.* **169**, 85–94 (2021).
44. Jampafuang, Y., Tongta, A. & Waiprib, Y. Impact of crystalline structural differences between α - and β -chitosan on their nanoparticle formation via ionic gelation and superoxide radical scavenging activities. *Polymers (Basel)*. **11**, (2019).
45. Cui, Z., Beach, E. & Anastas, P. Modification of chitosan films with environmentally benign reagents for increased water resistance. *Green Chem. Lett. Rev.* **4**, 35–40 (2011).
46. Mohandas, A. & Rangasamy, J. Nanocurcumin and arginine entrapped injectable chitosan hydrogel for restoration of hypoxia induced endothelial dysfunction. *Int. J. Biol. Macromol.* **166**, 471–482 (2021).
47. Cai, B. *et al.* Preparation, characterization and in vitro release study of drug-loaded sodium carboxy-methylcellulose/chitosan composite sponge. *PLoS One* **13**, e0206275 (2018).
48. Fan, X. *et al.* Morphology-controllable cellulose/chitosan sponge for deep wound hemostasis with surfactant and pore-foaming agent. *Mater. Sci. Eng. C* **118**, 111408 (2021).
49. Cheng, H. *et al.* Facile preparation of polysaccharide-based sponges and their potential application in wound dressing. *J. Mater. Chem. B* **6**, 634–640 (2018).
50. Moukbi, Y. *et al.* Biohydrogels for medical applications: A short review. *Org. Commun.* **11**", 123–141 (2018).
51. Gilaberte, Y., Prieto-Torres, L., Pastushenko, I. & Juarranz, Á. Anatomy and Function of the Skin. in *Nanoscience in Dermatology* 1–14 (Elsevier Inc., 2016). doi:10.1016/B978-0-12-802926-8.00001-X.
52. Wang, L.-P. *et al.* Preparation of stretchable composite film and its application in skin burn repair. *J. Mech. Behav. Biomed. Mater.* **113**, 104114 (2021).
53. Capanema, N. S. V *et al.* Superabsorbent crosslinked carboxymethyl cellulose-PEG hydrogels for potential wound dressing applications. *Int. J. Biol. Macromol.* **106**, 1218–1234 (2018).
54. Song, K., Zhu, W., Li, X. & Yu, Z. A novel mechanical robust, self-healing and shape

- memory hydrogel based on PVA reinforced by cellulose nanocrystal. *Mater. Lett.* **260**, 126884 (2020).
55. El Fawal, G. F., Abu-Serie, M. M., Hassan, M. A. & Elnouby, M. S. Hydroxyethyl cellulose hydrogel for wound dressing: Fabrication, characterization and in vitro evaluation. *Int. J. Biol. Macromol.* **111**, 649–659 (2018).
 56. Liu, R., Dai, L., Si, C. & Zeng, Z. Antibacterial and hemostatic hydrogel via nanocomposite from cellulose nanofibers. *Carbohydr. Polym.* **195**, 63–70 (2018).
 57. Shefa, A. A. *et al.* Curcumin incorporation into an oxidized cellulose nanofiber-polyvinyl alcohol hydrogel system promotes wound healing. *Mater. Des.* **186**, 108313 (2020).
 58. Gonzalez, J. S., Ludueña, L. N., Ponce, A. & Alvarez, V. A. Poly(vinyl alcohol)/cellulose nanowhiskers nanocomposite hydrogels for potential wound dressings. *Mater. Sci. Eng. C* **34**, 54–61 (2014).
 59. Koneru, A., Dharmalingam, K. & Anandalakshmi, R. Cellulose based nanocomposite hydrogel films consisting of sodium carboxymethylcellulose–grapefruit seed extract nanoparticles for potential wound healing applications. *Int. J. Biol. Macromol.* **148**, 833–842 (2020).
 60. Rakhshaei, R. & Namazi, H. A potential bioactive wound dressing based on carboxymethyl cellulose/ZnO impregnated MCM-41 nanocomposite hydrogel. *Mater. Sci. Eng. C* **73**, 456–464 (2017).
 61. Villalba-Rodríguez, A. M., Dhama, K. & Iqbal, H. M. N. Biomaterials-based hydrogels and their drug delivery potentialities. *International Journal of Pharmacology* vol. 13 864–873 (2017).
 62. Grabowski, P. Physiology of bone. *Endocrine Development* vol. 16 32–48 (2009).
 63. Buck, D. W. & Dumanian, G. A. Bone biology and physiology: Part I. the fundamentals. *Plastic and Reconstructive Surgery* vol. 129 1314–1320 (2012).
 64. Valtanen, R. S., Yang, Y. P., Gurtner, G. C., Maloney, W. J. & Lowenberg, D. W. Synthetic bone tissue engineering graft substitutes: What is the future? *Injury* (2020)

doi:10.1016/j.injury.2020.07.040.

65. Ulrich-Vinther, M., Maloney, M. D., Schwarz, E. M., Rosier, R. & O’Keefe, R. J. Articular Cartilage Biology. *JAAOS - J. Am. Acad. Orthop. Surg.* **11**, (2003).
66. Chocholata, P., Kulda, V. & Babuska, V. Fabrication of Scaffolds for Bone-Tissue Regeneration. *Mater. (Basel, Switzerland)* **12**, 568 (2019).
67. Polo-Corrales, L., Latorre-Esteves, M. & Ramirez-Vick, J. E. Scaffold design for bone regeneration. *J. Nanosci. Nanotechnol.* **14**, 15–56 (2014).
68. Zheng, Z. *et al.* Surface properties of chitosan films modified with polycations and their effects on the behavior of PC12 cells. *J. Bioact. Compat. Polym.* **24**, 63–82 (2009).
69. Wei, W. *et al.* Advanced hydrogels for the repair of cartilage defects and regeneration. *Bioactive Materials* vol. 6 998–1011 (2021).
70. Zou, Z. *et al.* Simultaneous incorporation of PTH(1–34) and nano-hydroxyapatite into Chitosan/Alginate Hydrogels for efficient bone regeneration. *Bioact. Mater.* **6**, 1839–1851 (2021).
71. Maharjan, B. *et al.* Regenerated cellulose nanofiber reinforced chitosan hydrogel scaffolds for bone tissue engineering. *Carbohydr. Polym.* **251**, 117023 (2021).
72. Ghorbani, M., Roshangar, L. & Soleimani Rad, J. Development of reinforced chitosan/pectin scaffold by using the cellulose nanocrystals as nanofillers: An injectable hydrogel for tissue engineering. *Eur. Polym. J.* **130**, 109697 (2020).
73. Khoylou, F. & Naimian, F. Radiation synthesis of superabsorbent polyethylene oxide/tragacanth hydrogel. *Radiat. Phys. Chem.* **78**, 195–198 (2009).
74. Glassford, S. E., Byrne, B. & Kazarian, S. G. Recent applications of ATR FTIR spectroscopy and imaging to proteins. *Biochimica et Biophysica Acta - Proteins and Proteomics* vol. 1834 2849–2858 (2013).
75. Perkinelmer. FTIRATR. https://www.perkinelmer.com/CMSResources/Images/44-74844TCH_FTIRATR.pdf (2021).
76. Misra, N. N., Sullivan, C. & Cullen, P. J. Process Analytical Technology (PAT) and

- Multivariate Methods for Downstream Processes. *Curr. Biochem. Eng.* **2**, 4–16 (2015).
77. Gill, P., Moghadam, T. T. & Ranjbar, B. Differential scanning calorimetry techniques: Applications in biology and nanoscience. *Journal of Biomolecular Techniques* vol. 21 167–193 (2010).
 78. Rouquerol, F., Rouquerol, J. & Llewellyn, P. Thermal Analysis. in *Developments in Clay Science* vol. 5 361–379 (Elsevier B.V., 2013).
 79. Stark, W. & Bohmeyer, W. Non-destructive evaluation (NDE) of composites: Using ultrasound to monitor the curing of composites. in *Non-Destructive Evaluation (NDE) of Polymer Matrix Composites: Techniques and Applications* 136–181 (Elsevier Ltd, 2013). doi:10.1533/9780857093554.1.136.
 80. Leyva-Porras, C. *et al.* Application of Differential Scanning Calorimetry (DSC) and Modulated Differential Scanning Calorimetry (MDSC) in Food and Drug Industries. *Polymers* vol. 12 (2020).
 81. Gun'ko, V. M., Savina, I. N. & Mikhalovsky, S. V. Properties of Water Bound in Hydrogels. *Gels (Basel, Switzerland)* **3**, (2017).
 82. Hassan, C. M. & Peppas, N. A. Structure and morphology of freeze/thawed PVA hydrogels. *Macromolecules* **33**, 2472–2479 (2000).
 83. Kaliva, M. & Vamvakaki, M. Nanomaterials characterization. in *Polymer Science and Nanotechnology* 401–433 (Elsevier, 2020). doi:10.1016/B978-0-12-816806-6.00017-0.
 84. Chusuei, C. C. & Goodman, D. W. X-Ray Photoelectron Spectroscopy. in *Reference Module in Chemistry, Molecular Sciences and Chemical Engineering* (Elsevier, 2013). doi:10.1016/B978-0-12-409547-2.05460-3.
 85. Sudhanshu, R. *X-RAY PHOTOELECTRON SPECTROSCOPY (XPS) TECHNOLOGY*. (2020).
 86. Zou, S. & Liu, T. *Fundamentals of X-Ray Photoelectron Spectroscopy (XPS)*. (2020).
 87. Rob. XPS. <http://www.rowbo.info/XPS.html> (2021).
 88. SathishKumar, R., Arthanareeswaran, G., Ismail, A. F., Abdullah, M. S. & Cheer, N. B.

- Nuclear Magnetic Resonance (NMR) Spectroscopy. in *Membrane Characterization* 69–80 (Elsevier Inc., 2017). doi:10.1016/B978-0-444-63776-5.00004-8.
89. Levitan, A. NMR Spectroscopy. (2014).
 90. Encyclopedia of Spectroscopy and Spectrometry - 3rd Edition. <https://www.elsevier.com/books/encyclopedia-of-spectroscopy-and-spectrometry/lindon/978-0-12-803224-4>.
 91. Blümich, B. Low-field and benchtop NMR. *J. Magn. Reson.* **306**, 27–35 (2019).
 92. Hirai, A., Odani, H. & Nakajima, A. Determination of degree of deacetylation of chitosan by ¹H NMR spectroscopy. *Polym. Bull.* **26**, 87–94 (1991).
 93. Mohammed, A. & Abdullah, A. *Scanning Electron Microscopy (SEM): A Review*. (2019).
 94. Omid, M. *et al.* Characterization of biomaterials. in *Biomaterials for Oral and Dental Tissue Engineering* 97–115 (Elsevier Inc., 2017). doi:10.1016/B978-0-08-100961-1.00007-4.
 95. Susan Swapp. Scanning Electron Microscopy (SEM). *Scanning Electron Microscopy (SEM)* https://serc.carleton.edu/research_education/geochemsheets/techniques/SEM.html (2017).
 96. Zhou, W., Apkarian, R., Wang, Z. L. & Joy, D. Fundamentals of scanning electron microscopy (SEM). in *Scanning Microscopy for Nanotechnology: Techniques and Applications* 1–40 (Springer New York, 2007). doi:10.1007/978-0-387-39620-0_1.
 97. Inkson, B. J. Scanning Electron Microscopy (SEM) and Transmission Electron Microscopy (TEM) for Materials Characterization. in *Materials Characterization Using Nondestructive Evaluation (NDE) Methods* 17–43 (Elsevier Inc., 2016). doi:10.1016/B978-0-08-100040-3.00002-X.
 98. Labcompare. Search | Labcompare.com. <https://www.labcompare.com/14-SearchResults/?search=stereomicroscope> (2021).
 99. Nothnagle, P., Chambers, W. & Davidson, M. Introduction to Stereomicroscopy. *MicroscopyU* 1–20

<https://www.microscopyu.com/techniques/stereomicroscopy/introduction-to-stereomicroscopy> (2013).

100. Weißpflog, J. *et al.* Characterization of chitosan with different degree of deacetylation and equal viscosity in dissolved and solid state – Insights by various complimentary methods. *Int. J. Biol. Macromol.* **171**, 242–261 (2021).
101. Focher, B., Beltrame, P. L., Naggi, A. & Torri, G. Alkaline N-deacetylation of chitin enhanced by flash treatments. Reaction kinetics and structure modifications. *Carbohydr. Polym.* **12**, 405–418 (1990).
102. Wojdyr, M. Fityk: A general-purpose peak fitting program. *J. Appl. Crystallogr.* **43**, 1126–1128 (2010).
103. Lavertu, M. *et al.* A validated ¹H NMR method for the determination of the degree of deacetylation of chitosan. *J. Pharm. Biomed. Anal.* **32**, 1149–1158 (2003).
104. Infrared and Raman Characteristic Group Frequencies: Tables and Charts. 3rd ed By George Socrates (The University of West London, Middlesex, U.K.). J. Wiley and Sons: Chichester. 2001. xviii + 348 pp. \$185.00. ISBN: 0-471-85298-8. *J. Am. Chem. Soc.* **124**, 1830 (2002).
105. Ibitoye, E. B. *et al.* Extraction and physicochemical characterization of chitin and chitosan isolated from house cricket. *Biomed. Mater.* **13**, (2018).
106. Martín-López, H. *et al.* Structural and Physicochemical Characterization of Chitosan Obtained by UAE and Its Effect on the Growth Inhibition of *Pythium ultimum*. *Agriculture* vol. 10 (2020).
107. Eddy, M., Tbib, B. & EL-Hami, K. A comparison of chitosan properties after extraction from shrimp shells by diluted and concentrated acids. *Heliyon* **6**, e03486 (2020).
108. Corazzari, I. *et al.* Advanced physico-chemical characterization of chitosan by means of TGA coupled on-line with FTIR and GCMS: Thermal degradation and water adsorption capacity. *Polym. Degrad. Stab.* **112**, 1–9 (2015).
109. Dharmalingam, K. & Anandalakshmi, R. Fabrication, characterization and drug loading

- efficiency of citric acid crosslinked NaCMC-HPMC hydrogel films for wound healing drug delivery applications. *Int. J. Biol. Macromol.* **134**, 815–829 (2019).
110. Karthikeyan, P., Banu, H. A. T., Preethi, J. & Meenakshi, S. Performance evaluation of biopolymeric hybrid membrane and their mechanistic approach for the remediation of phosphate and nitrate ions from water. *Cellulose* **27**, 4539–4554 (2020).
 111. Priyadarshi, R., Sauraj, Kumar, B. & Negi, Y. S. Chitosan film incorporated with citric acid and glycerol as an active packaging material for extension of green chilli shelf life. *Carbohydr. Polym.* **195**, 329–338 (2018).
 112. Wu, H. *et al.* Effect of citric acid induced crosslinking on the structure and properties of potato starch/chitosan composite films. *Food Hydrocoll.* **97**, 105208 (2019).
 113. Cai, B. *et al.* Preparation, characterization and in vitro release study of drug-loaded sodium carboxy-methylcellulose/chitosan composite sponge. *PLoS One* **13**, e0206275 (2018).
 114. Dong, Y., Ruan, Y., Wang, H., Zhao, Y. & Bi, D. Studies on glass transition temperature of chitosan with four techniques. *J. Appl. Polym. Sci.* **93**, 1553–1558 (2004).
 115. Sakurai, K., Maegawa, T. & Takahashi, T. Glass transition temperature of chitosan and miscibility of chitosan/poly(N-vinyl pyrrolidone) blends. *Polymer (Guildf)*. **41**, 7051–7056 (2000).
 116. Stevens, J. S. *et al.* Quantitative analysis of complex amino acids and RGD peptides by X-ray photoelectron spectroscopy (XPS). *Surf. Interface Anal.* **45**, 1238–1246 (2013).
 117. Machado, B. R. *et al.* Bactericidal Pectin/Chitosan/Glycerol Films for Food Pack Coatings: A Critical Viewpoint. *Int. J. Mol. Sci.* **21**, 8663 (2020).
 118. Liu, Y., Shen, X., Zhou, H., Wang, Y. & Deng, L. Chemical modification of chitosan film via surface grafting of citric acid molecular to promote the biomineralization. *Appl. Surf. Sci.* **370**, 270–278 (2016).
 119. Moreno-Vásquez, M. J. *et al.* Functionalization of chitosan by a free radical reaction: Characterization, antioxidant and antibacterial potential. *Carbohydr. Polym.* **155**, 117–127 (2017).

120. Gieroba, B. *et al.* Spectroscopic studies on the temperature-dependent molecular arrangements in hybrid chitosan/1,3- β -D-glucan polymeric matrices. *Int. J. Biol. Macromol.* **159**, 911–921 (2020).
121. Zhang, C., Zhang, H., Li, R. & Xing, Y. Morphology and adsorption properties of chitosan sulfate salt microspheres prepared by a microwave-assisted method. *RSC Adv.* **7**, 48189–48198 (2017).
122. Kong, Q., Wang, X. & Lou, T. Preparation of millimeter-sized chitosan/carboxymethyl cellulose hollow capsule and its dye adsorption properties. *Carbohydr. Polym.* **244**, 116481 (2020).
123. Capanema, N. *et al.* Eco-friendly and Biocompatible Crosslinked Carboxymethylcellulose Hydrogels as Adsorbents for the Removal of Organic Dye Pollutants for Environmental Applications. *Environ. Technol.* **39**, 1–42 (2017).

ANNEXES

ANNEX 1 List of reagents used

	Reagents	Description	Pictures
Dissolvent	Acetic acid	(CH_3COOH) MM REPRESENTATIONS	
Polymer matrix	CARBOXYMETHYL CELLULOSE SODIUM SALT HIGH VISCOSITY	$(\text{C}_8\text{H}_{15}\text{NaO}_8)$ LOBA Chemie CAS : 9004-32-4 CAS	
Polymer matrix	CHITOSAN	$(\text{C}_6\text{H}_{11}\text{O}_4)_n$ BioFinest	

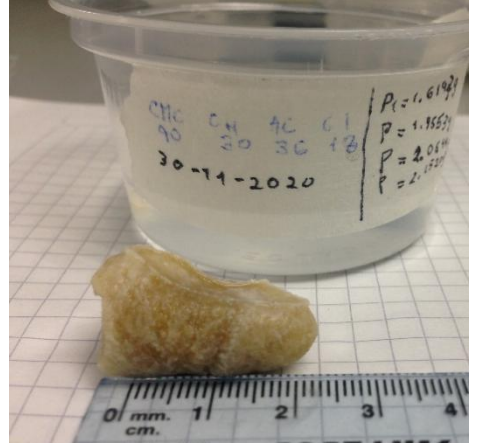
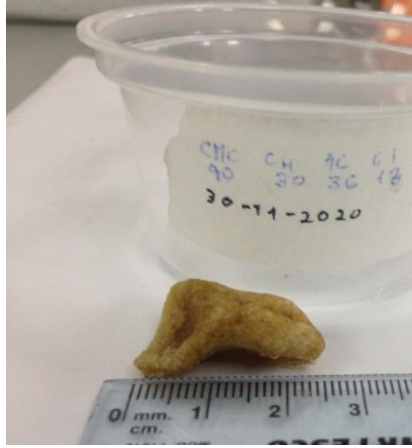
<p>Plasticizer</p>	<p>Glycerol</p>	<p>(C₃H₈O₃) SIGMA-ALDRICH CAS:56-81-5</p>	
<p>Plasticizer</p>	<p>Polyethylene glycol</p>	<p>C₂Nh₄n+2On+1 LOBA Chemie CAS:25322-68-3</p>	
<p>Crosslinker</p>	<p>Citric Acid anhydrous 99.5%</p>	<p>C₆H₈O₇ LOBA Chemie CAS: 77-92-9</p>	

ANNEX 2 Composites hydrogels with CH-A drying at room temperature dry state and swollen state after swelling 24 hours in 25ml of water

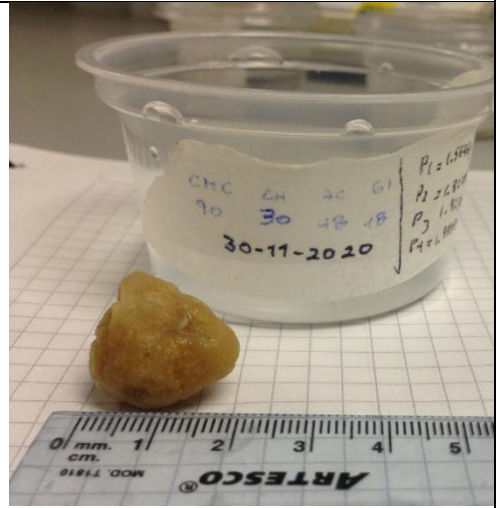
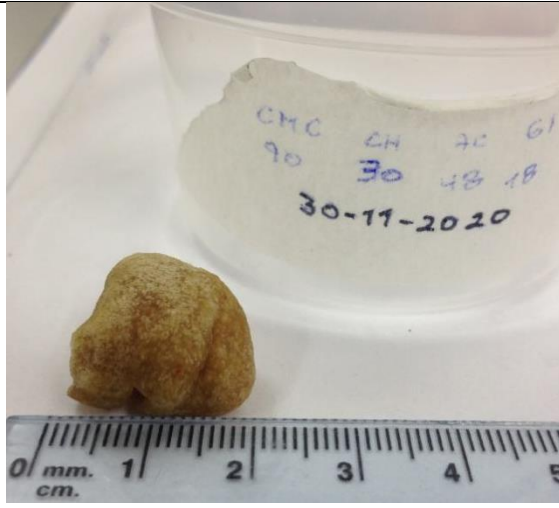
Code Composites hydrogels	Dry state	Swollen state
CMC/CH-A-CA24-G0	 <p>A photograph showing a small, irregular, yellowish-brown hydrogel in its dry state. It is placed on a white surface next to a ruler for scale. The ruler shows markings from 0 to 4 cm. In the background, a white container has a label with handwritten text: 'CMC 90 CH 30 AC 24' and '1-12-2020'.</p>	 <p>A photograph showing the same hydrogel after swelling in water for 24 hours. The hydrogel has significantly increased in size and is now a larger, more rounded, yellowish-brown mass. It is placed on a white surface next to a ruler for scale. The ruler shows markings from 0 to 5 cm. In the background, a white container has a label with handwritten text: 'CMC 90 CH 30 AC 24', '1-12-2020', and swelling ratios: 'P1 = 1.28', 'P2 = 1.64', 'P3 = 1.94', 'P4 = 1.68'.</p>
CMC/CH-A-CA36-G0	 <p>A photograph showing a small, irregular, yellowish-brown hydrogel in its dry state. It is placed on a white surface next to a ruler for scale. The ruler shows markings from 0 to 5 cm. In the background, a white container has a label with handwritten text: 'CMC 90 CH 30 AC 36' and '1-12-2020'.</p>	 <p>A photograph showing the same hydrogel after swelling in water for 24 hours. The hydrogel has significantly increased in size and is now a larger, more rounded, yellowish-brown mass. It is placed on a white surface next to a ruler for scale. The ruler shows markings from 0 to 5 cm. In the background, a white container has a label with handwritten text: 'CMC 90 CH 30 AC 36', '1-12-2020', and swelling ratios: 'P1 = 1.42', 'P2 = 1.70', 'P3 = 1.79', 'P4 = 1.87'.</p>

<p>CMC/CH- A-CA48-G0</p>		
<p>CMC/CH- A-CA96-G0</p>		
<p>CMC/CH- A-CA24- G18</p>		

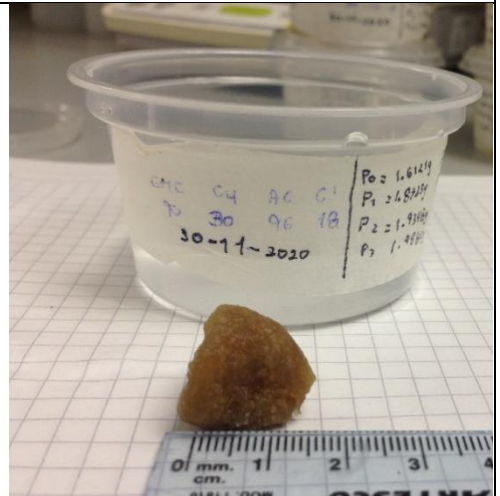
CMC/CH-
A-CA36-
G18



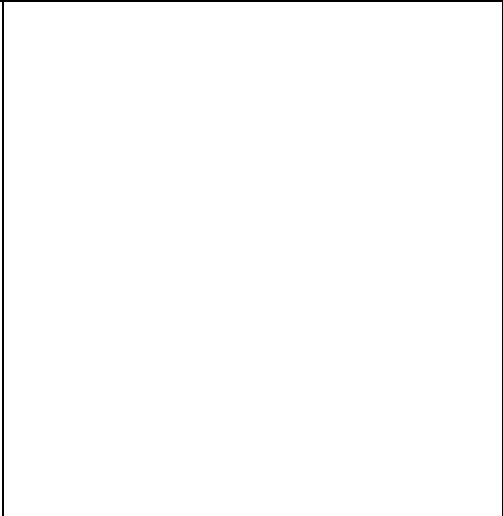
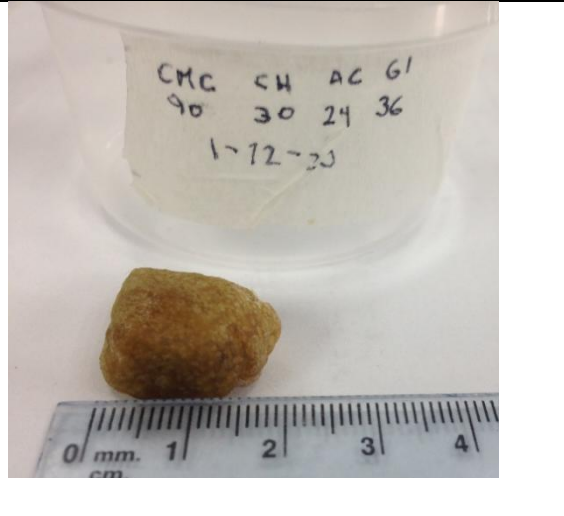
CMC/CH-
A-CA48-
G18



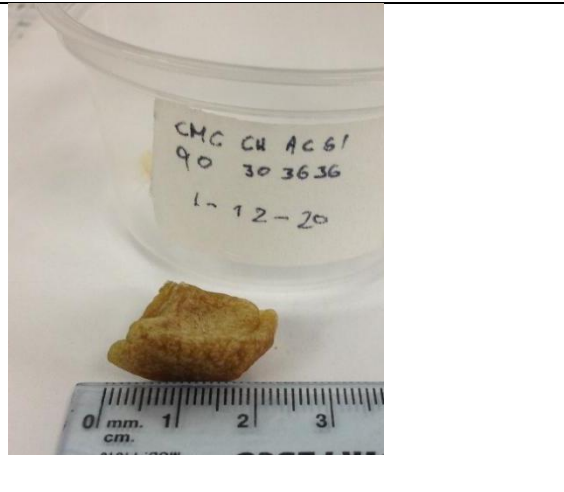
CMC/CH-
A-CA96-
G18



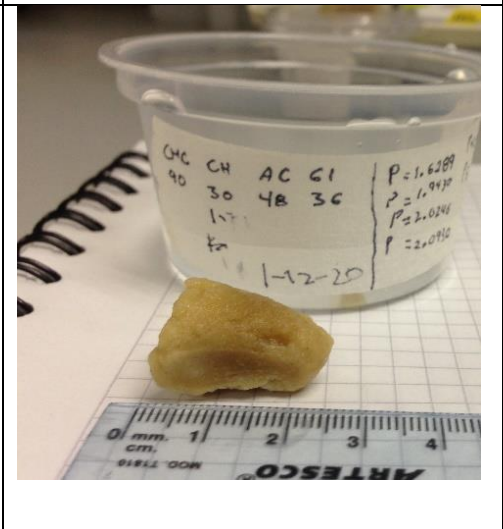
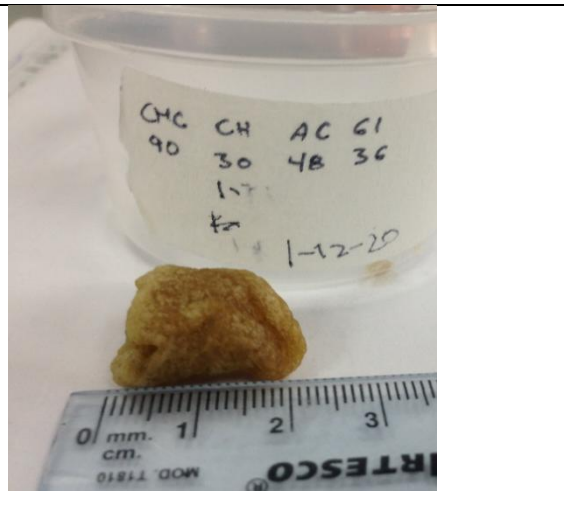
CMC/CH-
A-CA24-
G36



CMC/CH-
A-CA36-
G36



CMC/CH-
A-CA48-
G36



CMC/CH-
A-CA96-
G36

